Quaternary Science Reviews 116 (2015) 72–94

Contents lists available at ScienceDirect

Quaternary Science Reviews

journal homepage: www.elsevier.com/locate/quascirev

2700 years of Mediterranean environmental change in central Italy: a synthesis of sedimentary and cultural records to interpret past impacts of climate on society

Scott A. Mensing [a, *], Irene Tunno [b], Leonardo Sagnotti [c], Fabio Florindo [c], Paula Noble [d], Claire Archer [d], Susan Zimmerman [e], Francisco Javier Pavón-Carrasco [c], Gabriele Cifani [f], Susanna Passigli [f], Gianluca Piovesan [b]

[a] Department of Geography, University of Nevada, Reno, NV, USA
[b] Dendrology Lab, DAFNE Università degli Studi della Tuscia, Viterbo, Italy
[c] Istituto Nazionale di Geofisica e Vulcanologia, Rome, Italy
[d] Department of Geosciences, University of Nevada, Reno, NV, USA
[e] Center for Accelerator Mass Spectrometry, Lawrence Livermore National Laboratory, CA, USA
[f] Università degli Studi di Roma Tor Vergata, Rome, Italy

ARTICLE INFO

Article history:
Received 20 October 2014
Received in revised form
21 March 2015
Accepted 23 March 2015
Available online

Keywords:
Central Italy
Mediterranean environments
Society and climate
Paleoenvironmental change
Pollen
Paleomagnetism
Geochemistry
Historical documents
Late Holocene
Roman Empire

ABSTRACT

Abrupt climate change in the past is thought to have disrupted societies by accelerating environmental degradation, potentially leading to cultural collapse. Linking climate change directly to societal disruption is challenging because socioeconomic factors also play a large role, with climate being secondary or sometimes inconsequential. Combining paleolimnologic, historical, and archaeological methods provides for a more secure basis for interpreting the past impacts of climate on society. We present pollen, non-pollen palynomorph, geochemical, paleomagnetic and sedimentary data from a high-resolution 2700 yr lake sediment core from central Italy and compare these data with local historical documents and archeological surveys to reconstruct a record of environmental change in relation to socioeconomic history and climatic fluctuations. Here we document cases in which environmental change is strongly linked to changes in local land management practices in the absence of clear climatic change, as well as examples when climate change appears to have been a strong catalyst that resulted in significant environmental change that impacted local communities. During the Imperial Roman period, despite a long period of stable, mild climate, and a large urban population in nearby Rome, our site shows only limited evidence for environmental degradation. Warm and mild climate during the Medieval Warm period, on the other hand, led to widespread deforestation and erosion. The ability of the Romans to utilize imported resources through an extensive trade network may have allowed for preservation of the environment near the Roman capital, whereas during medieval time, the need to rely on local resources led to environmental degradation. Cool wet climate during the Little Ice Age led to a breakdown in local land use practices, widespread land abandonment and rapid reforestation. Our results present a high-resolution regional case study that explores the effect of climate change on society for an under-documented region of Europe.

1. Introduction

The extent to which past abrupt climate change has directly resulted in societal disruption or cultural collapse, and the ability of societies to adapt to these changes is strongly debated (Berglund, 2003; Diamond, 2005; Munoz et al., 2010), but is potentially significant for modern communities facing future climate change (Büntgen et al., 2011). Studies concerned with the link between climate and human affairs have increasingly recognized the need to examine societal change in parallel with climate change (Dearing et al., 2008; Coombes et al., 2009; Munoz et al., 2010; McCormick et al., 2012), although the tendency persists among physical

* Corresponding author.
E-mail address: smensing@unr.edu (S.A. Mensing).

http://dx.doi.org/10.1016/j.quascirev.2015.03.022
0277-3791/

scientists to link cultural shifts directly to climate change (O'Sullivan, 2008; Aimers, 2011). Detailed historical analyses based on precisely dated documents have identified instances when climate has led to significant societal disruption or 'collapse', but these analyses also detail multiple examples in which socioeconomic factors played the larger role in environmental change, with climate being secondary or inconsequential (Ladurie, 1971). For this reason, it is critical that studies attempting to elucidate the impact of climate on society closely couple paleoecologic methods with historical and archaeological methods (Dearing et al., 2008; O'Sullivan, 2008; Coombes et al., 2009; Harris, 2013).

The relationship between climate change and cultural response can be addressed in areas where multi-proxy studies of cores from lakes with very high sediment accumulation rates can be examined within the context of a well-documented written history (Berglund, 2003). Such a history may provide insights into human adaptive strategies that allowed societies to cope with past climate change (Fraser, 2011). Several recent high-resolution syntheses have drawn a link between climate stability and the expansion, and eventual contraction, of the Roman Empire (Büntgen et al., 2011; McCormick et al., 2012). These studies note that focused regional case studies with highly resolved datasets are still needed to test the potential effect of rapid climate change on human societies. Such datasets are particularly needed in under-documented regions of the Roman Empire, including southern Europe, and the regions near Rome.

In central Italy, archival materials are nearly continuously available from ~700 CE (common era) in the records of the Farfa Abbey (Leggio, 1995a) in northern Lazio, Central Italy, with some written records extending back to the Roman period (De Santis and Coarelli, 2009). These documents provide a written environmental history that can be compared with physical paleoecologic reconstructions. Paleoecologic reconstructions for the last 3000 years are still underrepresented in Italy (Roberts et al., 2004; Magri, 2007) with studies from the southern Alps and North Italy (Kaltenrieder et al., 2010; Joannin et al., 2014), the northern and central Apennines (e.g. Mercuri et al., 2002; Brown et al., 2013; Branch and Marini, 2014), the Tiber Delta (Di Rita et al., 2010), and southern Italy, Sicily and Sardinia (e.g. Russo Ermolli and di Pasquale, 2002; Di Rita and Magri, 2009; Tinner et al., 2009; Di Rita and Melis, 2013; Sadori et al., 2013). These studies record the major changes in vegetation in relation to human activity during this time period but present very different impacts depending on sites and historical periods. In addition, the sampling resolution is generally at the centennial or millennial scale and cannot be easily compared with historical records. The last 3000 years are of particular interest because they encompass several important climatic changes often associated with cultural change, including the Roman Optimum (100 BCE – 200 CE; BCE – before common era), the Medieval Warm Period (MWP), ~950 to 1250 CE, and the Little Ice Age (LIA) ~1250 to 1850 CE, (Büntgen et al., 2011; Christiansen and Ljungqvist, 2012; McCormick et al., 2012).

In this paper, we present multiple physical proxies (pollen, non-pollen palynomorphs, paleomagnetism, sedimentology, geochemistry and charcoal) from a small lake in the Rieti Basin, Central Italy, to reconstruct a high-resolution record of environmental history from the present through the pre-Roman period. The basin, located approximately 80 km north of Rome, has a well-documented archeological record from pre-Roman times (Coccia et al., 1992) and historical documents from early Roman times (Coccia et al., 1992; Leggio, 1995a). We compare our physical proxies with the well-documented historical record of human activity and cultural change, and with independent climate records to explore the link between the timing of climate change, environmental change, and historical events. This study complements previous high-resolution regional syntheses from central and northern Europe (Ladurie, 1971; Büntgen et al., 2011; McCormick et al., 2012) by providing a new site in southern Europe at the center of the Roman Empire. The results contribute to our understanding of Mediterranean forest dynamics and can be used to verify recent efforts to model the history of deforestation in Europe (Kaplan et al., 2009).

2. Study area

Lago Lungo (369 m above mean sea level) is one of four remnant lakes of ancient *Lacus Velinus* in the Rieti Basin (Fig. 1), an intermontane depression in the Central Apennines that locally reach an elevation of 2217 m at Monti Reatini (Calderoni et al., 1994). The Velino, Salto and Turano Rivers flow into the basin, which is then drained by the Velino River, which plummets over a travertine sill at Marmore Falls. Other sources of inflow into the basin are numerous artesian springs that lie along the eastern edge of the basin. Water level in the basin is controlled by the elevation of the travertine sill (Calderoni et al., 1994). During prehistoric time, travertine built up during warm periods, raising the sill and expanding wetlands, and alternatively eroded during cold periods draining the valley (Calderini et al., 1998; Soligo et al., 2002). Between ~6000 and 3000 yr BP a large shallow lake (*Lacus Velinus*) filled the basin (Calderoni et al., 1994). Written documents suggest that the Romans cut a channel through the travertine sill to drain the land in ~270 BCE (Coccia et al., 1992). Since that time, water level in the basin has been controlled periodically by maintaining existing channels and cutting new channels (Lorenzetti, 1989). Historical maps suggest that the size and shape of lakes, their proximity to the Velino River, and the extent of wetlands in the basin has changed through time. Today, Lago Lungo has a maximum depth of up to 7 m with a surface area of 0.78 km^2 and surface level maintained at 369 m above sea level (Riccardi, 2006). Inflow is from a network of ditches that drain surrounding wetlands, springs, and farmland. Lago Lungo is protected within Riserva Naturale dei Laghi Lungo e Ripasottile (Riccardi, 2006).

The geology of the region is characterized by recently uplifted marine sediments. The Central Apennines are primarily composed of Upper Triassic to Middle Miocene carbonates (Parotto and Praturlon, 1975; Cosentino et al., 2010). Rieti is a seismically active extensional basin within the Apennine thrust system and is partially filled with Upper Pliocene and Holocene continental and marine sediments (Cavinato and De Celles, 1999; Soligo et al., 2002). Travertine outcrops are present across the basin, associated with past periods of warm wet climate. Seismic activity has influenced the location and discharge of springs responsible for depositing the travertines (Soligo et al., 2002). The largest spring in the basin, Santa Susanna Spring, has a discharge of 4.1 $m^3 s^{-1}$ and is located ~3 km northeast of Lago Lungo (Spadoni et al., 2010).

Modern vegetation is dominated by agriculture in the basin and heavily managed forest on the surrounding slopes. *Phragmites* and *Salix* species grow in a narrow (~15 m) band of protected land within the reserve, while beyond the reserve border the basin floor is nearly entirely devoted to agriculture (Casella et al., 2009). Forest vegetation at lower elevations within the basin is characterized by temperate deciduous forest (e.g. *Carpinus betulus* L., *Fraxinus* spp., *Ulmus campestris* Auct.) with an important submediterranean component (*Quercus pubescens* Willd., *Quercus cerris* L.; *Carpinus orientalis* Miller; *Ostrya carpinifolia* Scop.); in the foothills on steep/shallow soils some patches of Mediterranean trees and shrubs (*Quercus ilex* L., *Phyllirea variabilis* L., *Pinus halepensis* Miller) are present while in the mountain belt (above 800–900 m) beech (*Fagus sylvatica* L.) forests are common. Climatically the area is within a transition zone between warm and cool temperate climates with a Mediterranean precipitation pattern characterized by low precipitation during summer. Mean annual temperature varies

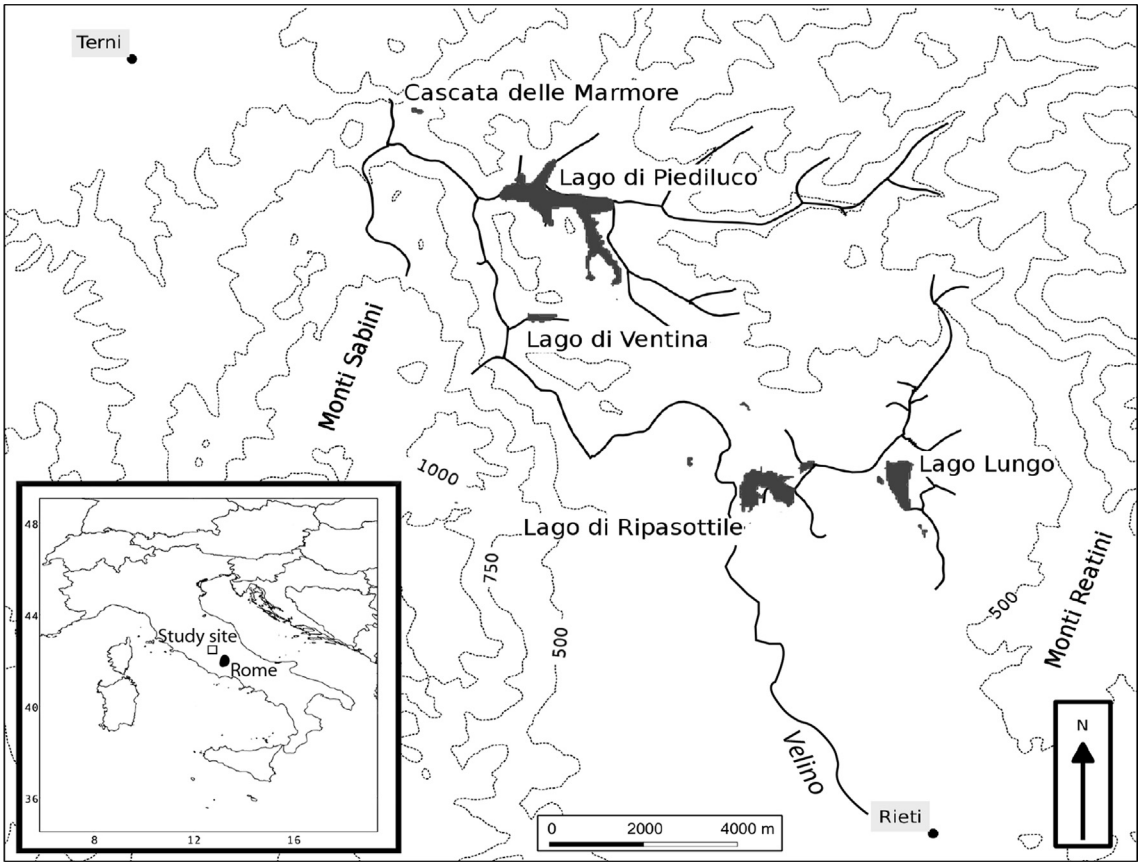

Fig. 1. Rieti Basin study site map.

between 4 °C in January and 21 °C in July with annual precipitation of 1117 mm (Fig. 4.29 in Leone, 2004). The general temperature and precipitation regime is strongly controlled by the North Atlantic Oscillation (NAO) with warm dry climate predominating during positive phases of the NAO, and cool wet climate during negative phases (Hurrell, 1995; Piovesan and Schirone, 2000; López-Moreno et al., 2011).

3. Materials and methods

3.1. Core recovery

Previous studies of Lago Lungo recovered cores on land near the lakeshore using geologic drilling equipment and subsequently did not recover the upper sediments containing the last few thousand years (Calderoni et al., 1994). For this study, we worked on a floating platform anchored near the center of the lake. Cores were collected in 2009 and in 2012. Water depth at the core site was 4.2 m in 2009 and 4.4 m in 2012. Surface sediments were obtained using a clear plastic tube fitted with a piston to recover the sediment–water interface (core LUN12-2C). The unconsolidated surface sediments were stabilized with Zorbitrol (sodium polyacrylate absorbent powder) while the core was still in an upright position. Overlapping cores (LUN09 in 2009 and LUN12-1A, 1B, 2A, and 2B in 2012) were recovered with a modified square-rod Livingstone hand operated corer, extruded directly into rigid ABS (Acrylonitrile Butadiene Styrene) plastic tubing, and capped for transport.

LUN09 spanned sediment depths from 54 to 605 cm and was recovered in six sections. We used GPS to relocate the LUN09 core site in 2012 for taking the next set of cores. Cores LUN12-1A and 1B were taken within 2 m of each other and spanned from 10 to 870 cm depth (ten sections) and 60–1028 cm depth (twelve sections) respectively. Cores LUN12-2A, 2B and 2C were taken ~10 m from the other set and within 2 m of each other. LUN12-2A spanned from 60 to 1300 cm depth (fifteen sections) and LUN12-2B, the longest core, from 20 to 1438 cm depth (nineteen sections). LUN12-2C, the surface core, contains the sediment–water interface to 123 cm depth.

LUN-09 was described, analyzed and stored at the Tuscia University Paleoecology Laboratory in Viterbo, Italy. Cores LUN12-1A and 1B were transported to the Tuscia University Paleoecology Laboratory for storage and subsequent u-channel sampling for paleomagnetic analyses. Cores LUN12-2A, 2B- and 1C were shipped to the United States National Lacustrine Core Facility (LacCore) in Minneapolis, Minnesota for initial core description, sampling for pollen, charcoal, smear slide and LOI analysis, and permanent storage.

3.2. Initial core description and analysis

Core LUN09 was split, photographed and the sediments described in July, 2009. This core was used for pollen analysis of the upper 5 m of core. Cores LUN12-2A, 2B and 2C were first logged whole using a Geoteck Multisensor Core Logger to measure density, acoustic wave velocity, electrical resistivity and loop-sensor magnetic susceptibility at 1-cm resolution. Cores were then split, the surface cleaned, imaged with a digital line scanner at ~300 dpi, then placed on a Geotek MSCL-XYZ core scanner and measured at 0.5-cm resolution for magnetic susceptibility and color. Magnetic susceptibility data and core images were input into an electronic

standard core description sheet and the sheets annotated for stratigraphy, sedimentology and correlation points between cores using both the images and the freshly split cores. Smear slides, taken every 20 cm and from selected strata, were used to aid in core description and to identify the major sedimentologic components.

The observed sedimentologic features and magnetic susceptibility data were used to correlate cores LUN12 2A, 2B, and 2C, often allowing for a visual match of individual suites of bands and layers between cores (Figs. 2 and 3). Areas of core distortion, caused by coring artifacts, and sections with no core recovery were identified, and a continuous 'master core,' hereafter referred to as LUN12-2, was constructed from the three cores, that spans a total sedimentary thickness of 14.4 m. Magnetic susceptibility was further used to correlate between core LUN12-2 and LUN12-1A and 1B, and LUN09, which were neither photographed nor logged in detail.

Samples (1.25 cm^3) were taken every 10 cm (3–5 cm in sediment transition zones) from LUN12-2 for measuring percent total organic matter (%organic) and percent carbonate (%$CaCO_3$) using the loss on ignition method protocols at LacCore based on Dean (1974) and Heiri et al. (2001). Samples were weighed, dried at 100 °C for 24 h, then combusted at 550 °C for four hours followed by combustion at 1000 °C for two hours.

Core LUN12-2 was transported to the Large Lakes Laboratory in Duluth, Minnesota for analysis using the ITRAX x-ray fluorescence (XRF) scanner (Cox Analytical Instruments) to provide elemental geochemistry data. The LUN12-2 core was scanned at a resolution of 0.5 cm throughout, except for the middle 7 sections (2B-5L through 11L), which were scanned at a resolution of 0.2 cm to pick up observed variations in sedimentary banding. The top section (LUN12-2C) was also scanned at a 0.2 cm resolution. The scanner was operated using a molybdenum source, 30 s dwell-time, a voltage of 30 kV and an x-ray current of 30 mA to obtain peak areas for elements Si–Pb. A principal component analysis using the rda function in the vegan 2.0-6 package in R, version 2.1.5.2 (R Development Core Team, 2012) was performed on the raw XRF data output, on both the whole core and on individual sections as an initial data analysis step to determine gross distribution patterns and co-variance of elements. Time series plots for core LUN12-2 were then generated for a subset of elements determined to be of interest as sedimentologic and lake chemistry proxies (Ti, Fe, Mn, Ca, and Sr). Raw counts of the element subset were normalized by centering and standardizing the data (raw data-mean of data/standard deviation), allowing for the comparison of the minima, maxima, and trends of major elements with very different ranges of counts within the core.

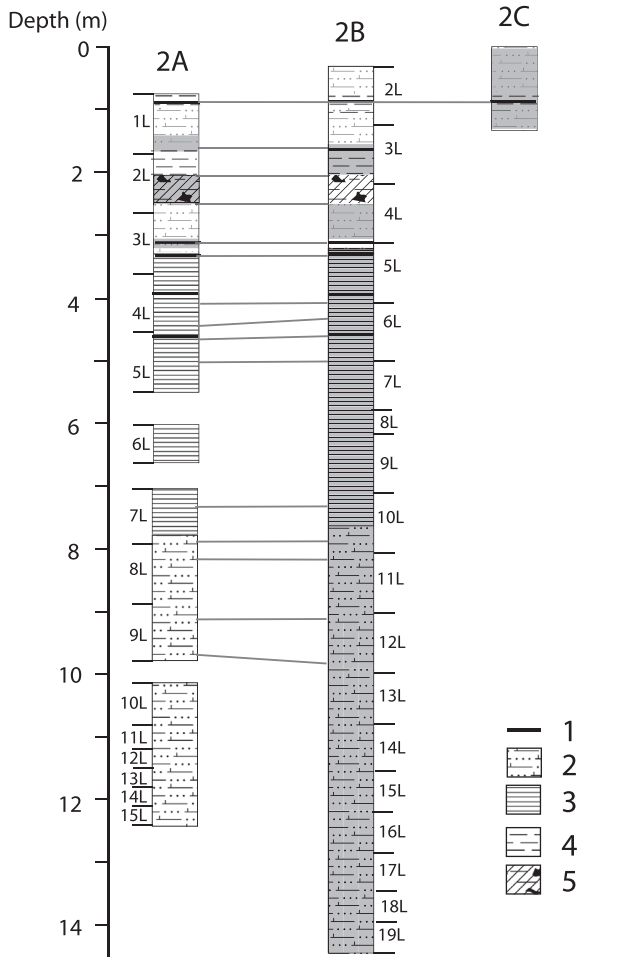

Fig. 2. Correlation of cores 2A, 2B, and 2C based distinctive sedimentologic features. Livingston core sections are denoted for cores 2A and 2B. Shaded areas denote sections used in composite core, pictured in Fig. 3. 1 = oxidized band; 2 = discontinuously laminated dark silty marl; 3 = varicolored banded clay, silt, and carbonate; 4 = gray clay; 5 = organic-rich marl with calcite stringers.

3.3. Rock magnetism and paleomagnetism

Natural and artificial magnetizations were measured at room temperature at the paleomagnetic laboratory of the Istituto Nazionale di Geofisica e Vulcanologia (INGV) in Rome, on a narrow-access (45 mm diameter) automated pass through '2G Enterprises' DC 755 superconducting rock magnetometer (SRM), housed in a Lodestar Magnetics shielded room. The cryogenic magnetometer is equipped with in-line orthogonal alternating field (AF) demagnetization coils, with optional application of a single-axis direct current (DC) field for production of an anhysteretic remanent magnetization (ARM). Rock magnetic and paleomagnetic properties were measured at 1-cm spacing on u-channel samples collected from 4 distinct and partly overlapping cores (LUN09, LUN12-1A, LUN12-1B and the lower 5.4 m of LUN12-2B).

To minimize sample dehydration and alteration, u-channel samples were stored in a refrigerated room until they were processed. For each u-channel, we first measured both the low-field magnetic susceptibility (κ), using a Bartington magnetic susceptibility probe MS2C in-line with the rock magnetometer, and the natural remanent magnetization (NRM). Then, all u-channels were AF demagnetized in 10 steps (using peak fields of 5, 10, 15, 20, 30, 40, 50, 60, 80 and 100 milliTesla (mT), with remanence vectors measured after each demagnetization step, in order to investigate the stability of the NRM and to reveal possible secondary overprints.

Finally, an ARM was imparted using a 0.05 mT direct current (DC) bias field and an axial 100 mT peak AF, and translating the u-channel through the AF and dc coil system at a speed of 10 cm/s, the lowest speed allowed by the software running the measurements. The adopted procedure equals an AF decay rate of ca 67 μT/half-cycle and results in the highest ARM intensity achievable with the employed instrumental setting and management software (Sagnotti et al., 2003; Sagnotti, 2013). The ARM was then measured and stepwise AF demagnetized using the procedure applied to the NRM.

From the AF demagnetization data of both the NRM and the ARM we computed the median destructive field (MDF), which is defined as the value of the peak AF necessary to reduce the remanence intensity to half of its initial value.

The raw magnetic moment data measured by the three orthogonal SQUID sensors of the SRM system were automatically corrected by compensating for the different shape and widths of

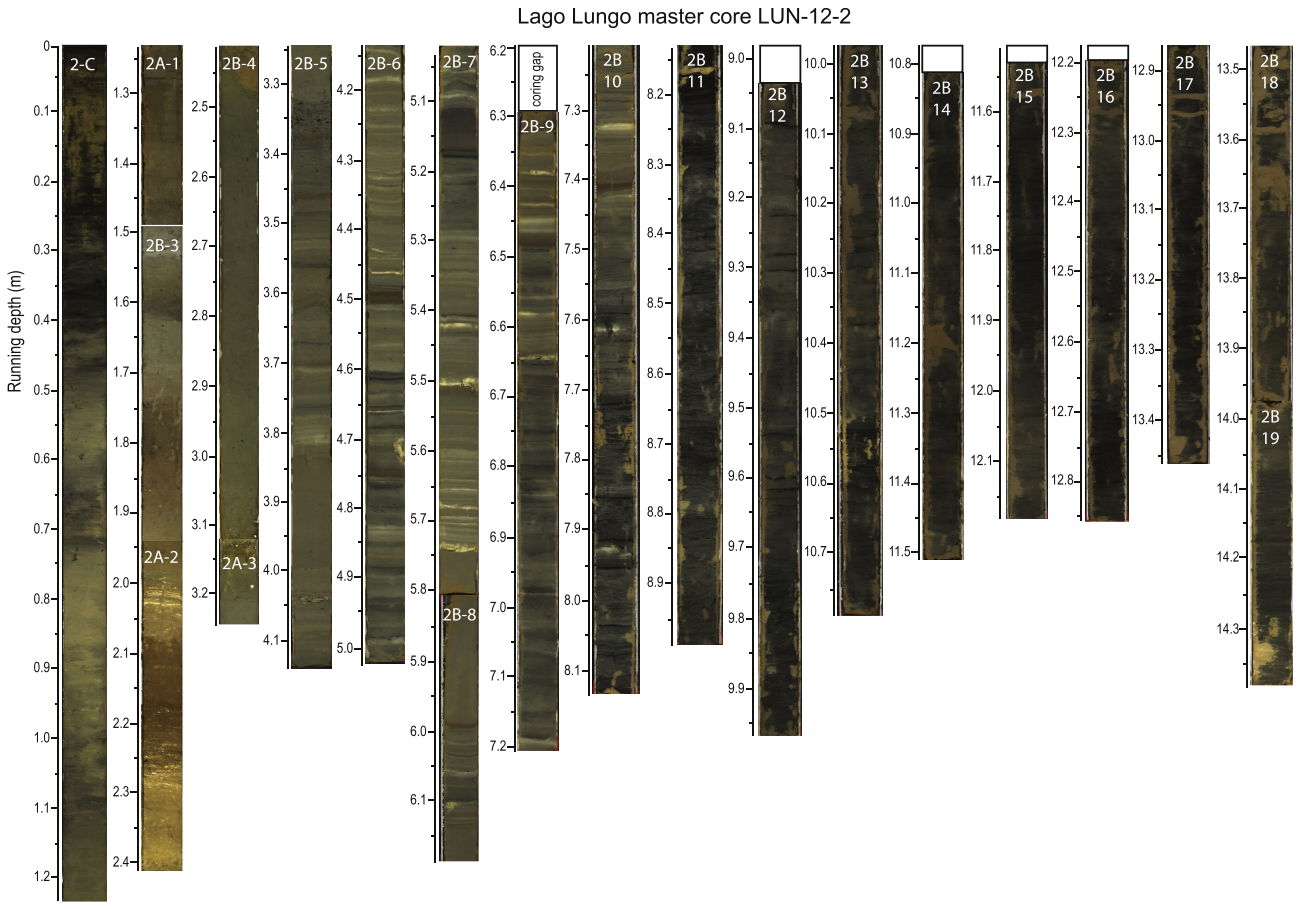

Fig. 3. High resolution images of the Lago Lungo Master core (LUN 12-2). Individual cores sections used in the master are labelled. White boxes represent core sections with no recovery. Running depth is a continuous measure (m) of the total core length.

the response function curves of the three SQUID pick-up coils (Roberts, 2006). Moreover, we took particular care in avoiding eventual disturbance effects that may be introduced during the coring, cutting and sampling procedures and could result in remanence deflections due to plastic deformation of the soft sediments. We also disregarded the paleomagnetic data for ~5 cm at both ends of each u-channel to avoid disturbances linked to edge effects.

3.4. ^{210}PB, ^{137}CS, and ^{14}C AMS analysis

Continuous 1-cm^3 samples were taken from the full length of the surface core (LUN12-2C), freeze dried and sent to Flett Research Ltd. for ^{210}Pb and ^{137}CS analysis. Plant macrofossils for ^{14}C AMS dating were not found during the initial core description, therefore extensive efforts were made to obtain datable materials. To find plant macrofossils and macroscopic charcoal, we sieved a total of 525 cm of core (90 samples, 5 from LUN09 and 85 from LUN12). For LUN09 we subsampled 20-cm long sections of half the core (~200 cm^3 per sample), soaked the sediments in a 5% solution of sodium metaphosphate for 12 h, and then sieved at 250 μm. We followed the same process for LUN12 but decreased the sample size to 5-cm long sections (~50 cm^3). Two microscopic charcoal samples were picked by hand from samples that appeared to be richer in charcoal. We concentrated pollen from a 20 cm section of core for ^{14}C AMS dating, following Newnham et al. (2007) then purified the concentrate using flow cytometry (Tennant et al., 2013).

One macrofossil (LTL 4680A) was submitted for AMS analysis at CEDAD at the University of Salento, Brindisi, Italy; all others were submitted to the Center for Accelerator Mass Spectrometry (CAMS) at Lawrence Livermore National Laboratory, USA. All macrofossils were chemically pretreated with the standard acid-base-acid (ABA) treatment before being combusted under vacuum and graphitized according to standard procedures (Vogel et al., 1984).

To test for the magnitude of a potential aquatic reservoir effect, a *Phragmites* plant growing in the lake was uprooted and pieces of the roots, stem, and leaves were rinsed in deionized water before transport to LLNL for radiocarbon analysis. All samples were pretreated, graphitized, and measured according to the same protocols as the fossil samples; dates on the roots and leaves were replicated.

3.5. Tephra analysis

Italy has a history of active volcanic eruptions, although most are well to the south of our site and no tephras from the last three millennia have been confirmed for our region (Giaccio et al., 2009; Sulpizio et al., 2014). Nevertheless, to test the potential for tephrochronology, twelve 10–40 cm thick samples were collected from LUN12-1B at age intervals, based on the paleomagnetic secular variation age model, discussed below, corresponding to periods of eruptions from Vesuvius, Phlegrean Fields, Ischia Island, Vulcano and the Lipari Islands. Eight samples were prepared on alloy stubs for morphological and textural observations and qualitative chemical analysis of components using a Zeiss EVO MA 10 scanning

electron microscope (SEM) equipped with an Oxford ISIS microanalysis system at INGV in Pisa. No tephra were recovered and this line of investigation was not pursued further.

3.6. Pollen and charcoal analysis

A total of one hundred samples (0.625 cc volume) were processed for pollen analysis using acid digestion procedures (Faegri and Iversen, 1985); two samples from the surface core (LUN12-2C), forty from LUN09 (40–605 cm depth), and fifty-eight from LUN12-2B (460–1438 cm depth). A known quantity of an exotic tracer (*Lycopodium*) was added to each sample during processing (Stockmarr, 1971) and counted along with pollen for calculating pollen concentration. Pollen counts for LUN09 (6 m in length) were completed before recovering LUN12-2B (14.4 m in length), therefore we counted duplicate samples from each core for the overlapping section from 460 to 605 cm depth. Duplicate counts were similar, and in the overlapping section we used only the counts from LUN12-2B, which were done at a later date, for a total of ninety-one samples in the final pollen diagram. A minimum of 400 terrestrial pollen grains were counted per sample (mean = 441) except for samples with very low concentration rates (n = 23), in which case a sum of 200–300 grains were counted (mean = 222). Pollen count totals excluded aquatic pollen types, such as *Typha*, *Nuphar* and *Potamogeton*, algae, and non-pollen palynomorphs.

Pollen and non-pollen palynomorphs were identified using reference material in the Tuscia University Paleoecology Lab, published keys and manuscripts (Punt and Malotaux, 1984; Punt et al., 1991; Chester and Raine, 2001; Blackmore et al., 2003; Beug, 2004; van Geel and Aptroot, 2006; Cugny et al., 2010; van Geel et al., 2011). TC pollen (Taxaceae and Cupressaceae) was assumed to be *Juniperus*, a native taxa. Species of *Quercus* were identified as either *Q. pubescens – robur* L. type, or *Q. cerris* L. (deciduous) or *Q. ilex* L. (evergreen) following Van Benthem et al. (1984). For plotting purposes *Quercus* is represented as deciduous or evergreen (*Q. ilex* type). Members of the family Poaceae were identified as cereals if grains were >37 μm, pore diameter was >2.7 μm and annulus thickness was >2.0 μm, following Köhler and Lange (1979). Pollen percentages were calculated from the sum of terrestrial pollen, excluding indeterminate grains and *Cannabis* type (which was retted in the lake at certain periods). Accumulation rates (grains cm^{-2} yr^{-1}) were calculated by dividing concentration (grains cm^{-3}) by the number of years per sample (yr cm^{-1}) and normalizing by number of *Lycopodium* counted. Aquatic taxa, algae, and non-pollen palynomorphs are presented as accumulation rates, since they appear intermittently in the record and total quantity represents actual abundance better than does percentage. Zonation was interpreted from a constrained single-link dendrogram created using CONISS in the PolPal plotting program (Nalepka and Walanus, 2003). Data input included the fifty-three terrestrial taxa with at least one strata of >1% of the pollen sum, excluding *Cannabis* type and indeterminate grains.

Charcoal particles were counted on pollen slides in two size fractions, 50–125 um and >125 um –longest dimension (Sadori and Guardini, 2007). All fragments that met the criteria of being black and having a visible cellular structure were counted.

3.7. Archaeological, historical and archival documents

The bulk of the archaeological documentation is represented by two surveys carried out in the area in the 1980s by the University of Perugia and in the 1990s by the British School at Rome (Coccia et al., 1992, 1995).

The early medieval phase is well documented by one of the most important collections of Europe: the archive of the Farfa Abbey, which contains a body of documents concerning the history of the territory between the 8th and the 12th century AD. The late medieval phase (13th–15th century) is well documented through the archive of the Comune of Rieti and that of Rieti cathedral (Caciorgna, 1998, 2000; Leggio, 1998). The history from 16th century onward has been analyzed in detail by means of additional archive (Dupré, 1939; Lorenzetti, 1989) and map collections in the Archivio di Stato in Rome and Rieti (Lorenzetti, 1990, 1994, 2009). In correlating the sedimentary evidence with historical evidence we have provided names and time periods following the system developed by Coccia et al. (1995) based on changes in archeologic ceramics in the Rieti Basin.

4. Results and discussion

4.1. Chronology

Developing a core chronology based largely on ^{14}C dating proved challenging given that the carbonate bedrock introduces the potential for significant old-carbon effects and plant macrofossils were hard to find and not well-distributed throughout the core. We therefore developed two independent age models, one

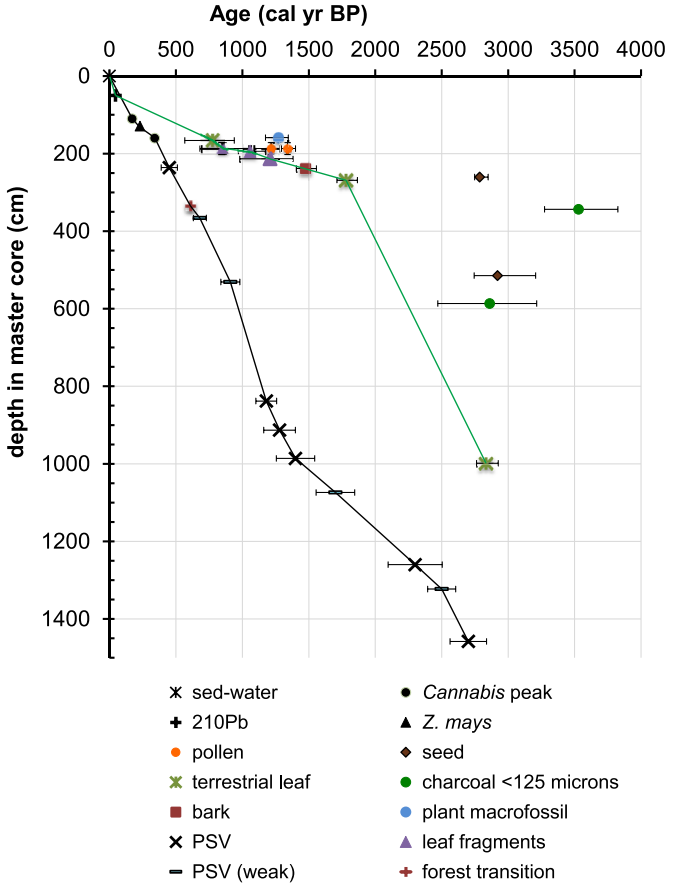

Fig. 4. Plot of all ^{14}C AMS radiocarbon and ^{210}Pb dates (Table 2) and PSV age model and cultigen dates (Table 1) used in this study. Black line represents the age model derived from PSV tie points including rock magnetic variables (RPI, inclination and declination) and cultigens (*Cannabis*, *Zea mays* and forest transition) described in Table 1. Green line represents the age model derived from ^{14}C on leaf fragments from LUN12 and ^{210}Pb basal date (Table 2). PSV uncertainties represent the 65% and 95% of confidence levels according to the SCHA.DIF.3k model predictions (Pavón-Carrasco et al., 2009). ^{14}C uncertainties represent the 2 sigma range of the mean probability using Calib 7.1 (Reimer et al., 2013). (For interpretation of the references to colour in this figure legend, the reader is referred to the web version of this article.)

Table 1
Tie points used in the PSV age model, including rock magnetic variables (RPI, inclination and declination) and cultigens (Cannabis, Zea mays, and forest transitions). Text in bold represent PSV features indicated with arrows in Fig. 7. Error on PSV ages is the 95% confidence interval according to the SCHA.DIF.3k model predictions (Pavón-Carrasco et al., 2009).

Run depth (cm)	Age BP (present = 2000)	Age CE/BCE	Error PSV data 95% (ca 2σ)	Notes
0	0	2000		Extrapolated
110	170	1830		Cultigen (end Cannabis peak)
134	250	1750		Cultigen (Zea mays first appearance)
160	340	1660		Cultigen (beginning Cannabis peak)
236	450	1550	61	**Inclination, Declination**
335	610	1390		Cultigen (transition from deforested to forested)
366	680	1320	49	RPI (weak evidence)
531	910	1190	71.5	RPI (weak evidence)
838	1180	820	78	**Inclination, RPI**
913	1280	720	119	**RPI**
986	1400	600	144.5	**Inclination, RPI**
1074	1700	300	145.5	RPI (weak evidence)
1260	2300	−300	203.5	**RPI**
1323	2500	−500	105.5	RPI (weak evidence)
1458	2700	−700	137.5	**Inclination, Declination**

based on historical documentation of biostratigraphic markers along with the information provided by the paleomagnetic secular variation (PSV), and another based on radiometric analyses (Fig. 4).

4.1.1. Biostratigraphic markers

Historical documentation of specific biotic changes within the basin (biostratigraphic markers we refer to as cultigens) were compared with the pollen reconstruction to provide estimated dates in the upper section of the core. *Zea mays* (corn) was introduced into Europe only after the first voyage of Columbus in 1492 CE. The first historical documents noting cultivation of *Z. mays* in Italy are from 1605 CE and most documents indicate that cultivation was initially sparse, introduced into central Italy after 1700 (Messedaglia, 1927). The first documented planting of *Z. mays* in the Rieti Basin is given as between 1740 and 1760 CE (De Felice, 1965; Covino, 1995) and we attribute a date of 1750 CE to the core depth (134 cm) with the first appearance of *Zea* pollen (Table 1).

Cannabis cultivation in the Rieti Basin for rope production expanded in the mid-17th century, peaked in the late 18th century, and eventually declined by the mid-19th century (Galli, 1840; Zuccagni-Orlandini, 1843; Nigrisoli, 1857; Celetti, 2007). The peak in Cannabis-type pollen (see Results Fig. 12) is coincident with the first appearance of *Zea* pollen. We designated a date of 1660 CE to the beginning of the rise in *Cannabis*-type pollen (160 cm), and a date of 1830 CE to the end (110 cm), a time when alternative fibers such as linen and cotton began replacing *Cannabis* across Europe (Lavrieux et al, 2013; see also Rull and Vegas-Vilarrúbia, 2014 for the rapid decline of hemp).

Reforestation associated with land abandonment following the Black Plague in 1349 CE depth has been documented repeatedly throughout Europe (van Hoof et al., 2006; Yeloff and van Geel, 2007; Sköld et al., 2010; Fraser, 2011). Written documents from Rieti described a similar pattern of land abandonment and reforestation towards the end of the 14th century (Leggio, 1995b; Naspi, 2010) and we gave a date of 1390 CE to the major transition from a deforested to forested landscape evident in the pollen record about 335 cm depth.

4.1.2. Paleomagnetic analysis

The measured rock magnetic properties (κ, NRM, ARM, MDF) were used to correlate cores LUN12 1A, 1B, 2A, 2B, 2C and LUN09 between overlapping sections and enabled us to build a composite magnetic section for the lake (Fig. 5). We constructed an age model based on the rock magnetic data and biostratigraphic cultigens described above.

The NRM demagnetization data allowed the unambiguous identification of a Characteristic Remanent Magnetization (ChRM) throughout all the sequence. The data indicate that the whole sequence is characterized by an almost single-component NRM, unambiguously isolated after removal of a weak viscous overprint in AF steps of 5–10 mT (Fig. 6). The orientation of the ChRM was defined by principal component analysis (Kirschvink, 1980) by fitting a line between the 10 and 50 mT AF demagnetization steps. The maximum angular deviation for each determined ChRM direction is 1° on average, with a full range of variation between 0.1° and 5°. The MDF of the NRM typically ranges between 15 and 40 mT indicating that magnetite is the main magnetic carrier in the sequence.

The ChRM declination of individual u-channels was arbitrarily rotated to align trends between adjacent sections. The stratigraphic trends in the ChRM declination and inclination are characterized by large amplitudes and high-frequency oscillations around the expected values for a geocentric axial dipole (GAD) field at the site. These wide oscillations and amplitudes are however unexpected, considering the recent models of paleosecular variation (PSV) of the geomagnetic field over the last millennia (Gallet et al., 2002; Pavón-Carrasco et al., 2009; Korte et al., 2011). In any case, these variations are consistent between the analyzed cores and the reconstructed ChRM directional trends are replicated in the overlapping sections of the distinct cores (Fig. 7).

To estimate relative paleointensity (RPI) variation, we normalized the NRM by κ and by the ARM intensity. The NRM/ARM ratio was computed also from the values measured after the 20 mT and 40 mT AF steps. All the normalization methods resulted in a similar pattern and therefore support a general coherency between the different normalization procedures and indicate a reliable reconstruction of the RPI trend. After removal of data affected by edge effects at the u-channel breaks, lithological boundaries and magnetic susceptibility spikes, the broadly smoothed paleomagnetic trends can be correlated to the available PSV curves and models for Europe: the directional (declination and inclination) archeomagnetic PSV curve (Gallet et al., 2002) built with a high quality archeomagnetic dataset from France, and the full geomagnetic field vector (declination, inclination and intensity) provided by the archeomagnetic SCHA.DIF.3k model of Pavón-Carrasco et al. (2009) (Fig. 7). This correlation enabled us to point out various depth-age tie-points from prominent PSV features.

In order to estimate the temporal error of the paleomagnetic tie-points we have calculated the temporal resolution of the regional model SCHA.DIF.3k at the geographic coordinates of Lago Lungo. For each tie-point, the three geomagnetic field elements, i.e.

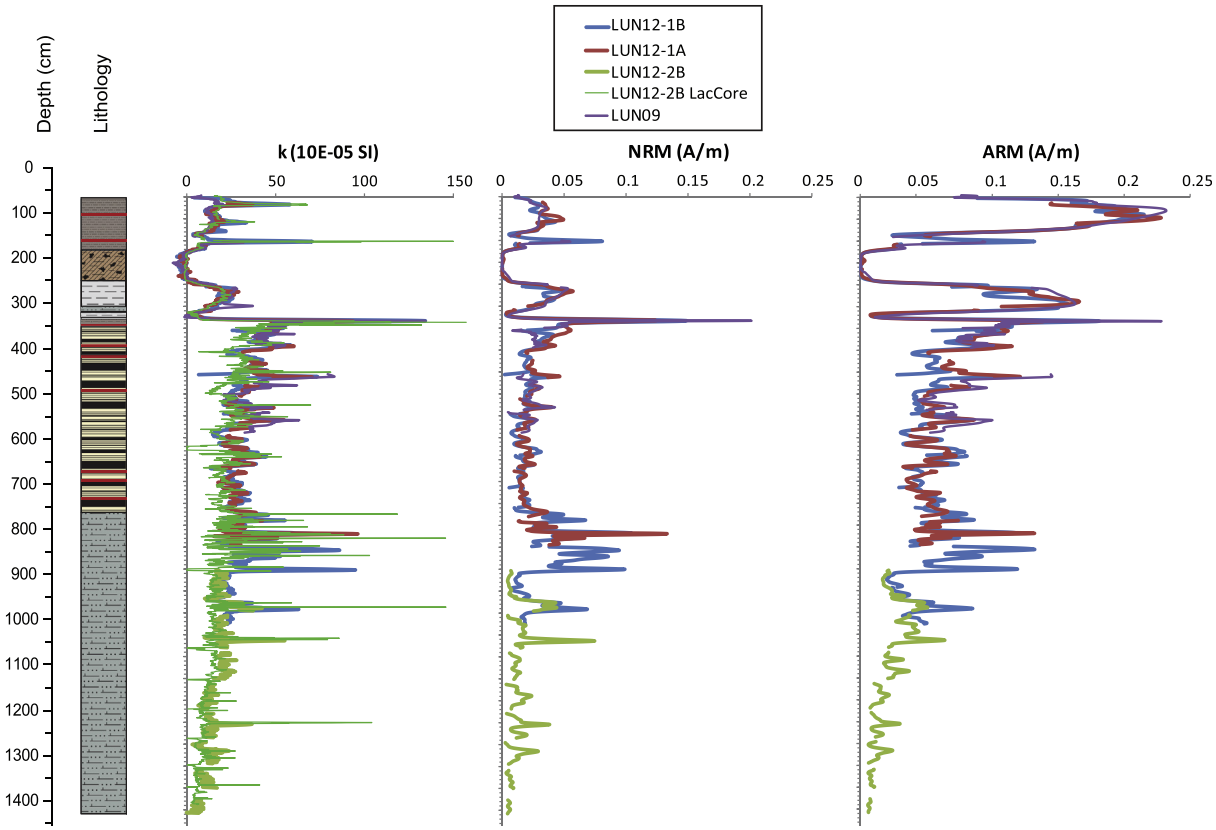

Fig. 5. Stratigraphic trends of k, NRM and ARM of the various cores, correlated to a common depth.

declination, inclination, and intensity, are defined by a temporal Probability Density Function (PDF). The PDF depends on the value of the geomagnetic field element at the corresponding time and its uncertainty (the α_{95} in the case of the directional elements and the intensity standard deviation, σ_F, for the intensities). The combination of the three PDFs for each geomagnetic element provides a final PDF which area allows us to calculate the minimum and maximum time for each tie-point. Then, the temporal resolution of the regional model is given by the difference of this maximum and minimum. Table 1 contains the paleomagnetic tie-points used in this study with the geomagnetic field elements and their uncertainties, at 95% confidence levels, according to the SCHA.DIF.3k model predictions (Pavón-Carrasco et al., 2009).

4.1.3. ^{210}PB, ^{137}CS, and ^{14}C AMS analysis

CS-137 activity was significantly above background for the core interval 24–41 cm with maximum activity at 28–29 cm depth, assumed to be 1963 CE. The CRS model of ^{210}Pb activity indicated an age of 1954 CE at 33.5 cm depth, and it was concluded that the CRS model provided a reasonable estimates of age in this core. The ^{210}Pb chronology produced a date of 1905 CE at 50.5 cm depth.

Fifteen radiocarbon dates were obtained from twelve depths in the LUN09 and LUN12-1B cores (Table 2 and Fig. 4). Sieving yielded six plant macrofossils and two macroscopic charcoal samples; all remaining plant macrofossils and microscopic charcoal were found during the sub-sampling process. Sorting of pollen by flow cytometry yielded 1.5 million pollen grains which were divided into two samples (of 900,000 and 600,000 pollen grain) to obtain replicate dates for the interval 172–202 cm in LUN09. The same interval yielded a sample of leaf fragments large enough to produce replicate radiocarbon dates. The leaf replicates produced essentially identical radiocarbon ages, but were significantly younger than the pollen replicates, by ~400 years. The pollen replicates are likely older because they integrate grains from the whole 30 cm sediment sample, whereas the leaves may represent a single depth of younger age.

The radiocarbon samples generally fit into two categories, based on their age and depth in the core. Between 1000 and 260 cm four samples have calibrated radiocarbon ages of ~2800 years cal yr BP, with a fifth (343 cm) dating to 3500 cal yr BP. Because of the similarity in age, despite a wide stratigraphic range, and the variety of materials (Table 2), it seems likely that these samples represent the occasional tapping of some remnant deposit formed at or before 2800 yr BP.

The second group of samples (n = 10) cluster between 266 and 159 cm, and produce radiocarbon ages ranging from 1800 to 780 cal yr BP. This second group also represents a wide range of sample types, and may be the result of a period of widespread and active erosion, caused by wetter overall climate or more intensive human disturbance of the landscape, or both. The two groups of dates overlap at ~260 cm depth.

We considered the relatively fragile uncharred leaf macrofossil ^{14}C dates (Table 2) the most reliable upon which to develop a radiometric chronology (Hatté et al., 2001). Although we were unable to identify leaf fragments to species, all appeared to be terrestrial. Macrofossils from core LUN-12 were considered more reliable than those from LUN-09 because they were recovered from 5-cm thick sections rather than 20 cm-thick sections. Since the sections from each core overlapped stratigraphically, we used the ^{14}C dates from leaf macrofossils in LUN-12 (Table 2, samples with

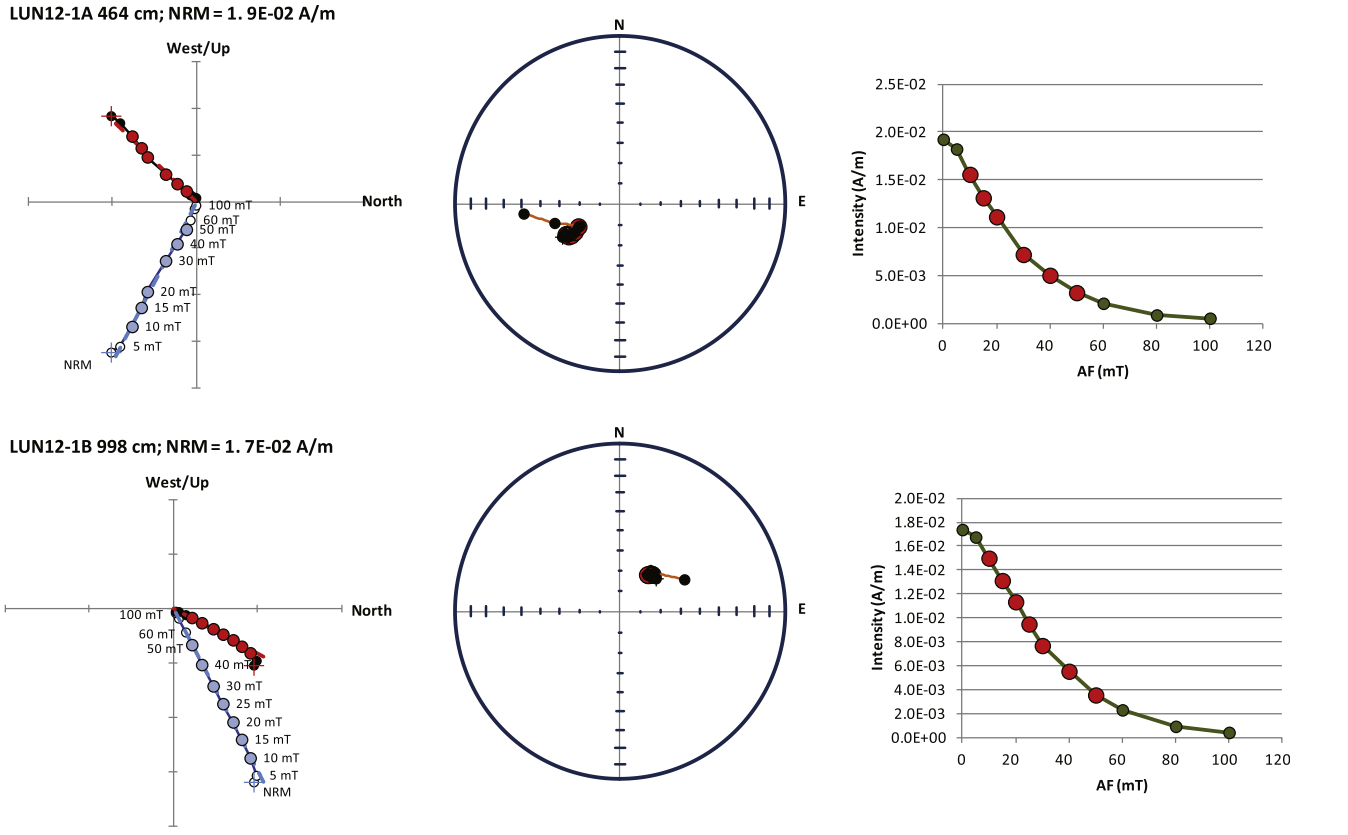

Fig. 6. Representative demagnetization diagrams analyzed with the DAIE workbook (Sagnotti, 2013). For the vector component diagrams, black (white) circles indicate projection on the horizontal (vertical) plane. When demagnetization steps are selected for PCA, the corresponding symbols turn to red (for horizontal projection) and to light blue (for vertical projections). The stereoplots are equal-area projections, with solid symbols representing points on the lower hemisphere. The plots showing the decay of the NRM intensity as a function of the demagnetization steps are shown on the right side of each equal-area projection.

center depths of 166, 193.5, 213.5, 238.5, 268.5, and 998.5 cm) in addition to the ^{210}Pb date (from 50.5 cm) to build an alternative age model.

4.1.4. Age model selection

To directly compare the two age models, we replotted the LUN-12 PSV data using the radiometric dates as tie points (Fig. 8), and compared this fit with the available PSV curves and models for Europe (Gallet et al., 2002; Pavón-Carrasco et al., 2009). Comparison of the two age models shows that the ^{14}C-based age model (Fig. 8) produces a poor fit between the LUN-12 PSV data and the PSV curves and models for Europe, especially when compared with the age model based on biostratigraphic markers and PSV tie points (Fig. 7). Note that each age model spans 3000 years, however in the ^{14}C-based model 3000 yr BP is at 10 m depth and in the PSV model this is at 14.4 m depth. The ^{14}C-based age model also produces age–depth relationships that are inconsistent with the written history. For example, the ^{14}C based age model gives a date of 1380 CE for the depth of 134 cm, the first occurrence of *Z. mays* pollen, a physical impossibility given the introduction history of that crop. The ^{14}C-based age model also results in dramatic changes in sedimentation rates at 268 cm depth from 6.92 to 0.96 mm yr^{-1}. Although this is physically possible, there is no indication in the appearance of the sediments (Fig. 3), or the geochemistry (Fig. 10) to support such a change at this depth. An organic rich interval occurs between 180 and 250 cm depth. The nature of the sediments, the magnetic properties and the geochemistry of this interval strongly indicate that it was deposited during a period of dramatically reduced terrigenous input in the basin. In the PSV based age model (Fig. 7) this interval would span about one century around 1530–1650 CE, a period of intense cold when historical maps indicate a very wide lake covering most of the basin. Conversely, in the ^{14}C based model (Fig. 8) this stratigraphic interval would correspond to about three centuries in the early medieval time (600–900 CE), a warm period for which historical sources indicate widespread forest cutting and therefore a greatly increased terrigenous input in the basin. Down core, further issues in interpreting the data emerge, including deforestation and draining of the basin by 400 BCE, more than a century before archaeological and written records suggest any Roman impacts.

Given the problems associated with the ^{14}C-based age model, we conclude that the PSV age model produces the most accurate chronology. In the PSV model, all three paleomagnetic measurements (inclination, declination and intensity) can be tied to the European PSV model through the full length of the core (Fig. 7), sedimentation rates do not change abruptly (Fig. 4), and the pollen record is consistent with known history. In addition, the ^{210}Pb date, although not used to create the model, was consistent with the model. In contrast, most of the ^{14}C ages fall within only one meter of the core. The clustering of macrofossils argues for the potential that macrofossils were transported to the lake irregularly, perhaps during a wet phase through flooding, erosion and redeposition of old materials. We do not have a complete explanation for the unusual ^{14}C dates, but radiocarbon dating of the different parts of the modern *Phragmites* shows that unidentified plant material that is from an aquatic plant might be 500 years too old (or more) (Table 2). Terrestrial plants that can grow in standing water (e.g.

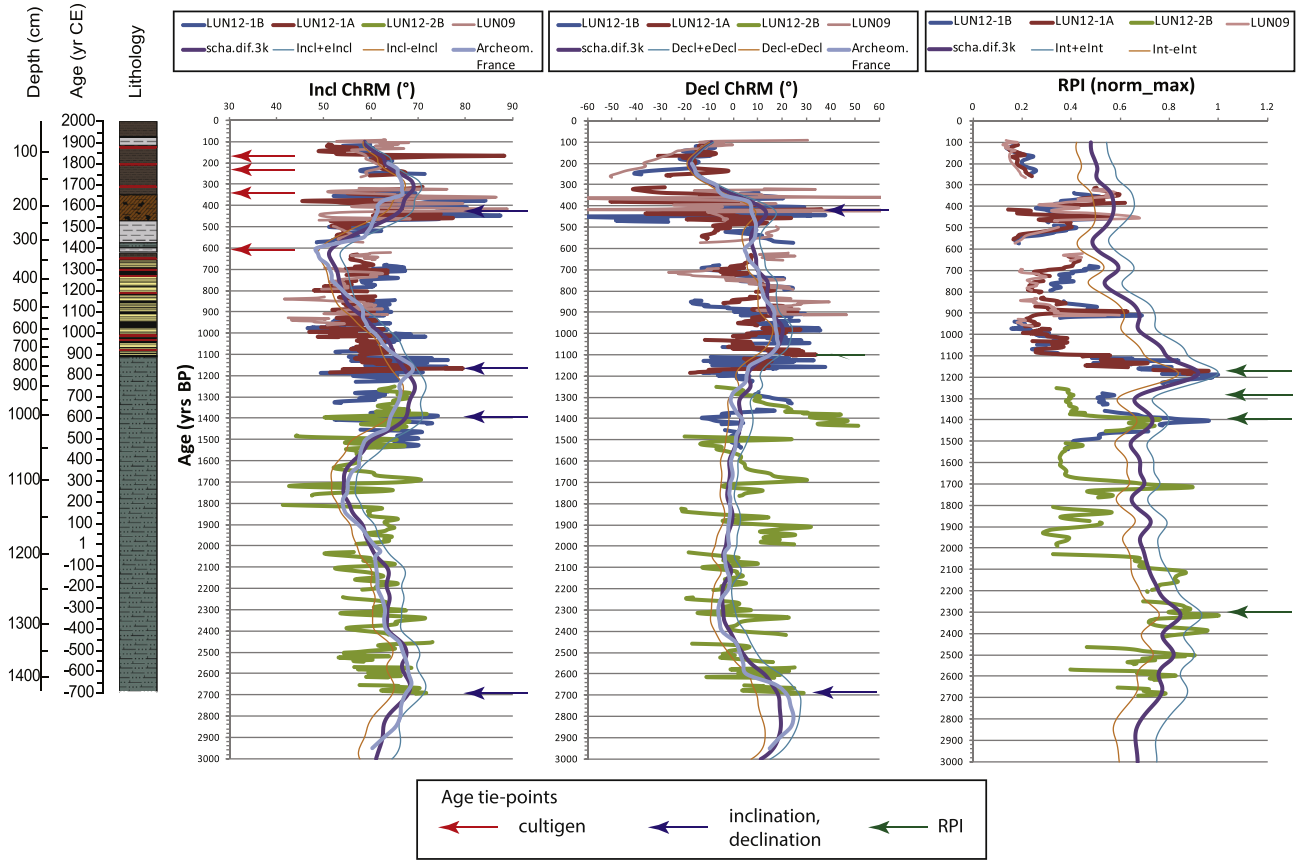

Fig. 7. PSV trends for the measured cores, plotted as a function of the common depth and age. Age was estimated by correlation with PSV reference curves and models (Archeomagnetic data from France, Gallet et al., 2002; scha.dif.3k of Pavón-Carrasco et al., 2009). Prominent PSV features (inclination, declination and RPI shown in bold in Table 1) used for depth vs age correlation and cultigens (significant changes in forest phase, and appearance of *Zea mays* and *Cannabis* type) from the pollen data are marked by arrows.

Salix) generally produce reliable ^{14}C dates (Hatté et al., 2001), and several of the dated samples were identifiably terrestrial, suggesting this is only a partial explanation. We intend to further explore the complexities of ^{14}C production and uptake within the study area.

4.2. Geochemical proxies

Several elements (Ca, Sr, Ti, Fe, Mn, and S) serve as proxies for siliclastic input, and authigenic or endogenic mineral fractions. The relationship of these elements can be seen in biplots of Principal Components 1 and 2 (Fig. 9), where the eigenvectors (red arrows) of the elements are superimposed over the data points, and 3 eigenvector trajectories (numbered 1, 2, and 3) are interpreted to have sedimentologic significance. The Medieval Period (MP) and Little Ice Age (LIA) intervals are plotted separately to show changes in elemental behavior between these two intervals (Fig. 9a, b). Ca is representative of the calcium carbonate ($CaCO_3$) component of the sediments, indicated by the good correlation between the Ca XRF and percent $CaCO_3$ derived from LOI (Fig. 10), and shows a distinct separate trajectory on the PCA plots (Fig. 9). Sr can co-precipitate with Ca as $SrCO_3$ when the lake waters are saturated with CO_3 (Haenssler et al., 2013), seen in the profile when Sr and Ca track together. Sr can also behave conservatively as a detrital element, tracking closely with Ti (Kylander et al., 2011). Ti is used in this study as a proxy for siliclastic detrital input into the lake (Haberzettl et al., 2008), controlled by erosion, weathering, and runoff within the catchment. Ti is representative of other conservative clastic elements such as K, Rb, and Zr that have near-identical profiles throughout the core, and are seen to have near identical eigenvectors with Ti (Fig. 9). Fe, while at times also behaving as a detrital element (Fig. 9b), is also influenced by redox processes and subject to remobilization at the sediment–water interface (Croudace et al., 2006). Mn is also influenced by redox processes, forming highly insoluble oxides in oxygenated conditions (Kylander et al., 2011) and is used here as an indication of changes in redox behavior of the upper few cm of the sediment. Mn shows a distinct trajectory in the PCA biplots, where Fe follows the behavior of Mn most closely in the MP (Fig. 9a). Sulfur shows an interesting profile and has been used as an indicator of evaporative balance and lake level changes, as it precipitates in chemically concentrated lake waters (Haenssler et al., 2013).

4.3. Core stratigraphy

Core stratigraphy is delineated by gross sedimentologic characteristics that are supplemented with petrographic observations, and time series curves of κ and geochemistry. The sequence is subdivided into four stratigraphic intervals that are assigned names based on their chronostratigraphic significance. The sedimentology of these intervals is described below.

4.3.1. Archaic through Early Medieval interval: 1438–800 cm, Age: 700 BCE–870 CE

This interval represents a number of historical periods (Coccia et al., 1995); including the Archaic (700–500 BCE), pre-Roman (500–300 BCE), Roman (300 BCE–400 CE), Late Antique (400–600 CE), and Early Medieval (600–800 CE) periods.

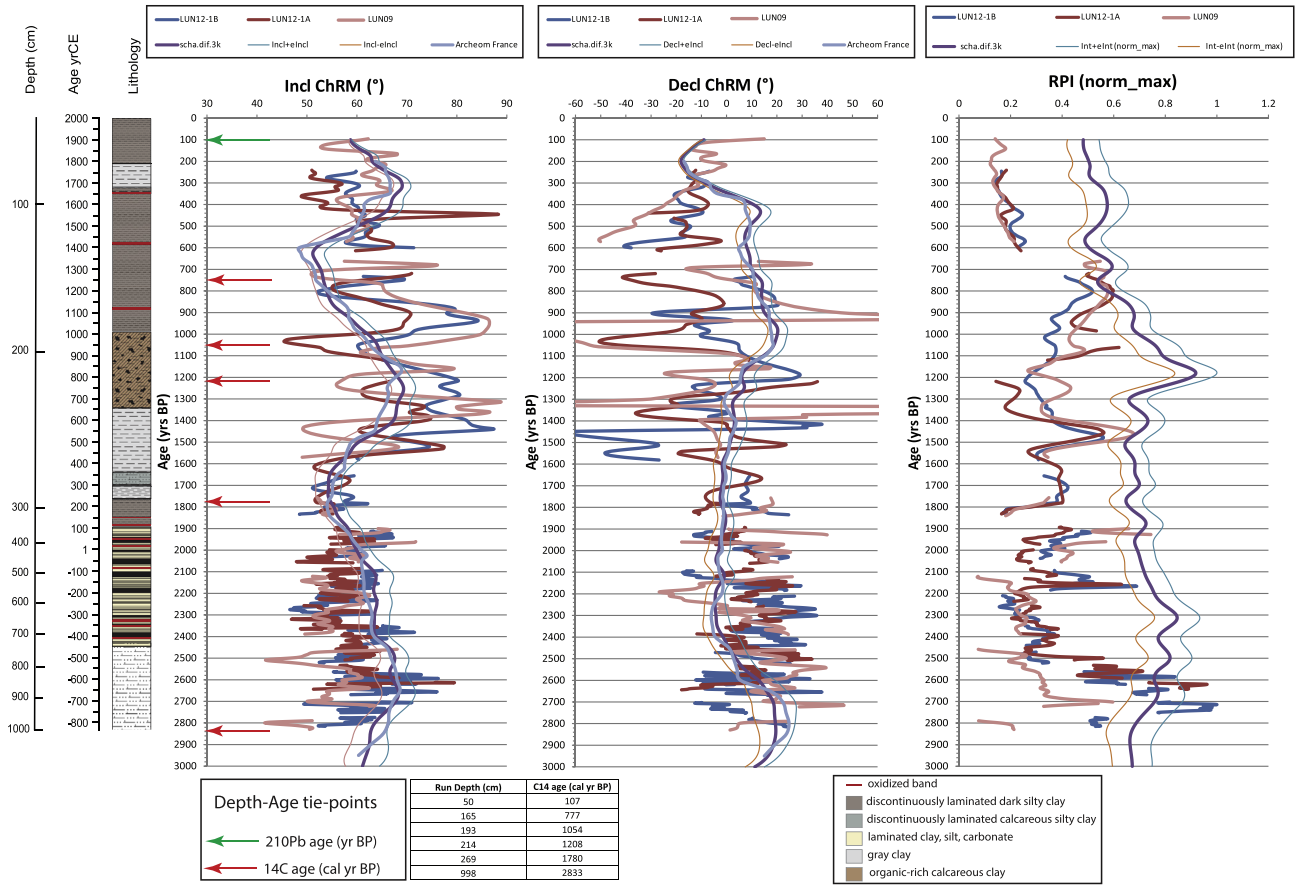

Fig. 8. PSV trends for core LUN-12-1A and 1B, plotted as a function of the ^{210}PB and ^{14}C AMS dates. In relation to the PSV reference curves and models (Archeomagnetic data from France, Gallet et al., 2002; scha.dif.3k of Pavón-Carrasco et al., 2009).

Table 2
Macrofossil ^{14}C dates for cores LUN09 and LUN12 and modern *Phragmites* plant. MAP is the median age probability. Min and max represent the 2 sigma error. Difference is the age difference between the PSV age model and ^{14}C age model graphed in Fig. 4. Dates marked with* are those used in the ^{14}C age model and indicated with arrows in Fig. 8.

Core	Depth (cm)	Lab ID	Material	^{14}C age	±	mg C	min (cal yr BP)	MAP (cal yr BP)	Max (cal yr BP)	MAP year CE	Difference cal ^{14}C-PSV
LUN12-1C	161–171	162752	Leaf fragment	840	100	0.036	567	777*	939	1175	543
LUN-09-1	172–202	152975	Leaf fragments	930	90		680	844	1048	1105	573
LUN-09-1	172–202	152973	Leaf fragments	960	60		737	859	965	1090	588
LUN12-1C	191–196	162753	Leaf fragments	1145	40	0.138	967	1054*	1171	895	771
LUN12-1C	211–216	162754	Leaf fragments	1300	100	0.039	981	1208*	1381	740	889
LUN-09-1	172–202	155264	Sorted pollen	1255	30	0.31	1085	1211	1277	740	940
LUN-09-1	172–202	155263	Sorted pollen	1445	40	0.19	1294	1340	1400	610	1069
LUN-09-1	158.5–159.5	LTL 4680A	Plant macro	1343	50		1174	1271	1345	680	1050
LUN12-1C	236–241	162755	Bark	1600	35	0.187	1406	1476	1557	475	1113
LUN12-1B	266–271	162767	Leaf fragments	1845	30	0.616	1712	1780*	1865	170	1363
LUN-09-1	260–261	152974	Seed	2680	35		2748	2785	2849	−835	2382
LUN12-1B	996–1001	162757	Leaf fragments	2745	35	0.275	2763	2833*	2925	−885	1108
LUN-09-1	586–587	152103	Charcoal	2730	130	0.03	2471	2861	3215	−910	1874
LUN12-1B	512–517	162756	Seed	2790	100	0.065	2744	2920	3207	−970	2062
LUN-09-1	343–344	152102	Charcoal	3290	100	0.04	3274	3530	3826	−1580	2979
		Modern phragmites		^{14}C age (yr BP)	±	mg C	Fraction modern	±	Cal yr BP (2-sig range)	year CE	
		162760	Leaf	>Modern		0.647	1.0158	0.0038	−5	1955	
		162758	Root	>Modern		0.610	1.0209	0.0039	−5	1955	
		163123	Root	>Modern		0.945	1.0238	0.0039	−5	1955	
		162759	Stem	540	30	0.836	0.9350	0.0033	515–560 598–632		
		163124	Stem	270	30	1.031	0.9668	0.0034	283–433		
				NH atmosphere in 2013, >40 deg N			1.057		0.0039		

All measured at CAMS-LLNL, except LTL 4680A, measured at CEDAD.
% all d13C values assumed to be −25 per mil, as per Stuiver and Polach (1977).

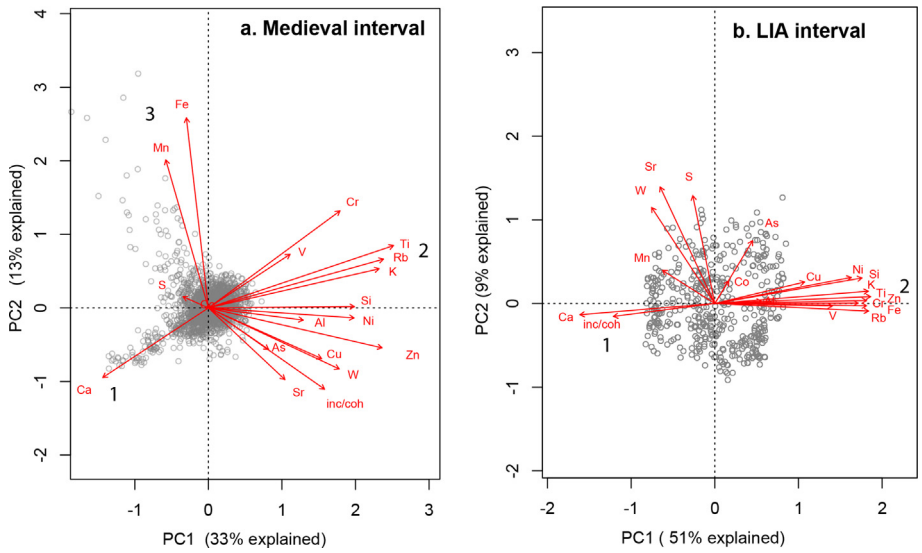

Fig. 9. Principal components analysis biplots for core 12LUN-2 showing variations in elemental composition from XRF data: a) Medieval interval and b) Little Ice Age interval. Samples are plotted as open circles and eigenvectors for elements in red. Axis 1 is largely related to carbonate (− values) versus siliciclastic (+values) component. 1) carbonate rich eigenvectors; 2) siliciclastic-rich eigenvectors; 3) redox eigenvectors. (For interpretation of the references to colour in this figure legend, the reader is referred to the web version of this article.)

Sedimentologically, the interval consists of a dark, discontinuously laminated, silty to clayey marl. The color is dark gray to black and fades to an olive color within hours of being exposed to air, indicating the presence of unstable monosulfides, or other redox-sensitive minerals in a reduced state. Small (<1 mm) black streaks in the core are aggregates of sub-micron-sized opaque black minerals within a clay matrix. Microscopic examination shows that the carbonate phase is significant (≥50%) in the form of calcite rhombohedrons (ranging from 2 to 20 μm), detrital carbonate allochems (<5 μm), *Phacotus* algal grains (5–10 μm), and rare fragments of Charophyte algae (>10 μm). The silt fraction is largely quartzofeldspathic, subangular, and occurs throughout, becoming an increasingly larger component towards the top of this interval. There is a diatom component (estimated at <10%) consisting predominantly of *cyclotelloid* phytoplankton with smaller amounts of araphid periphyton.

Some trends are observed in the lower and upper portions of this interval. At the base, the carbonate component is highest in the core and shows a gradual decline until 1250 cm (~300 BCE). This is indicated in both a decrease in Ca counts and %$CaCO_3$ determined

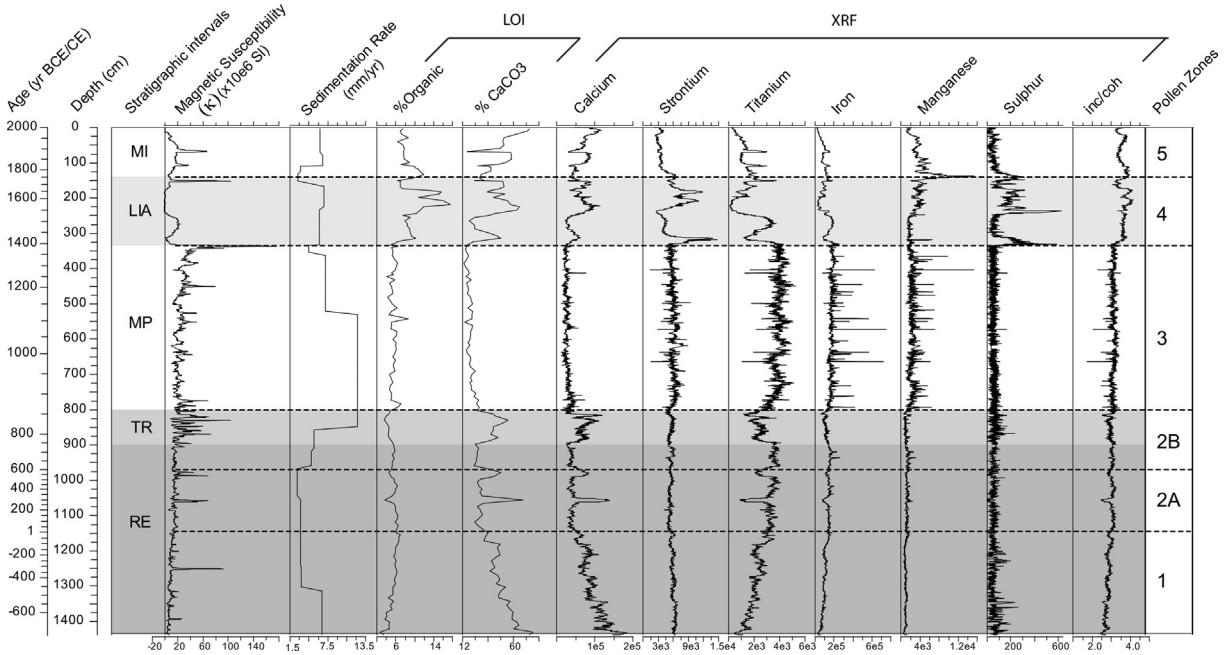

Fig. 10. Geochemical and sedimentological parameters, including Loss on Ignition data (LOI), magnetic susceptibility, selected elemental data from XRF (reported in kilacounts per second). Sediment accumulation rate was calculated from the age model. Stratigraphic intervals discussed in text are abbreviated on the left; Modern Interval (MI), Little Ice Age (LIA), Medieval Period (MP), Transitional Zone (TR) between MP and RE, and Roman Era and Migration Period (RE). Boundaries of pollen zones (dashed lines) listed on right are also discussed in the text.

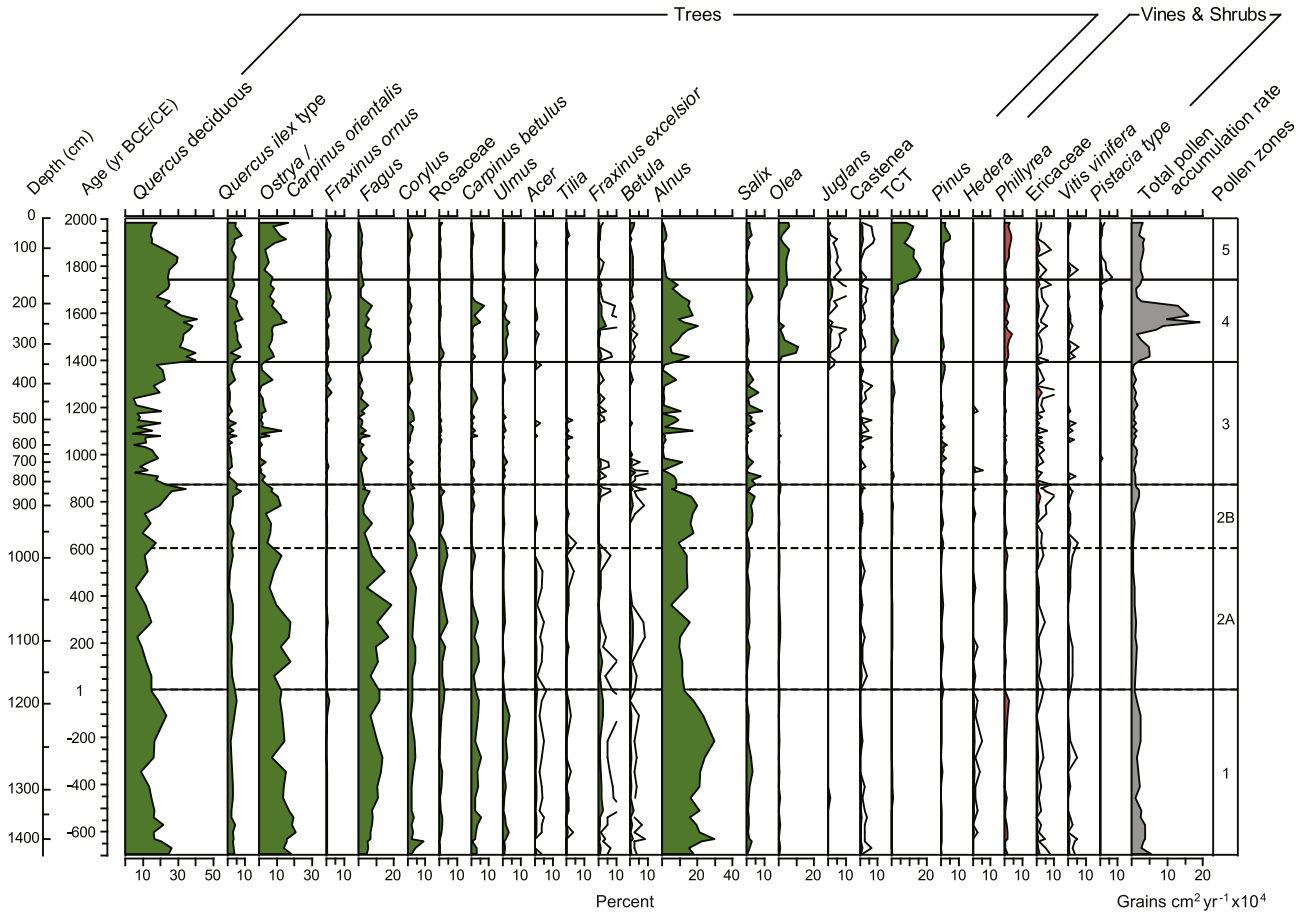

Fig. 11. Selected pollen taxa of trees, vines and shrubs, and total pollen accumulation rate. Unfilled lines represent 5X exaggeration.

by LOI, with a proportional increase in siliclastic components, as seen in the counts of Ti and Fe (Fig. 10). The κ has a baseline of ~10 E^{-5} SI, at the bottom of the core, then increases to ~20^{-5} sl, at 1150 cm reciprocating the decreased carbonate fraction. Sediment accumulation rates decrease with the drop in carbonate from ~7 mm yr^{-1} to the lowest rate in the core (~3 mm yr^{-1}). The top ~1 m of this interval, during the Early Medieval Period (875–800 cm; ~800–900 CE), shows some interesting sedimentological and geochemical features, although the distinction from the sediment below is not readily seen macroscopically in the core photos (Fig. 3). The κ signal shows large, frequent peaks above 100^{-5} SI (Fig. 10), sediment accumulation rate rapidly increases to ~12 mm yr^{-1} and there is a brief increase in carbonate content relative to siliciclastics. The uppermost ~45 cm, above 815 cm (870 CE), shows a large elemental shift commensurate with a decrease in organic matter and carbonate content. Diatoms are absent above 815 cm.

4.3.2. Medieval interval: 800–335 cm, Age: 870–1390 CE

This interval consists of gray thin bedded clay and silty–clay bands 1–30 mm thick, intercalated with varicolored reddish-brown, black, and buff-colored bands 2–10 mm thick. The reddish-brown to black layers appear to be rich in Fe and Mn, based on alignment of the core photos to the scanning XRF signal (Figs. 3 and 10). Fe and Mn show a close correspondence in the MP and have a similar eigenvector trajectory (Fig. 9a). The buff layers are 2–12 mm thick carbonate-rich bands that locally are hard and concretionary. Fine silty sand bands, 5–20 mm thick are interspersed throughout this interval, and contain as much as 80% quartzo-feldspathic grains. The carbonate fraction consists of small rhombohedrons, (2–5 μm), small detrital allochems (2–5 μm), *Phacodus* fragments (5–10 μm), and Charophyte fragments (10–80 μm). Sediment accumulation rates are high, a result of increased siliciclastic input, with correspondingly lower organic matter and carbonate fractions than the preceding interval. Diatoms are absent from this entire interval, with the exception of very rare fragmented or corroded frustules. The trends of the major elements, which shift dramatically at a core depth of 815 cm, persist throughout this interval. The top of this interval is marked by a very large κ peak not seen in the elemental data and a drop in sediment accumulation rate (Fig. 10).

4.3.3. Early Modern – Modern: 335–140 cm, Age: 1390–1740 CE

At a depth of 335 cm, the sedimentology of the shifts markedly. Siliciclastic content declines rapidly and then becomes variable, dominated by organic-rich calcareous material containing gastropod fragments and diatoms. Much of the organic matter appears to be aquatic in origin. Within this interval are two light yellowish zones rich in thin carbonate stringers and lenticular concretions. Petrographically, the carbonate is largely dendritic and ascicular, and of unknown genesis. A subordinate fraction of the carbonate is definitively algal, composed of Charophyte and *Phacodus* grains. Chemically, counts of siliciclastic elements (i.e. Ti) in this interval are the lowest in the core, and Ca and Sr have several maxima (Fig. 10). Mn and Fe are decoupled throughout this interval, and large peaks in S are observed for the first time, concurrent with

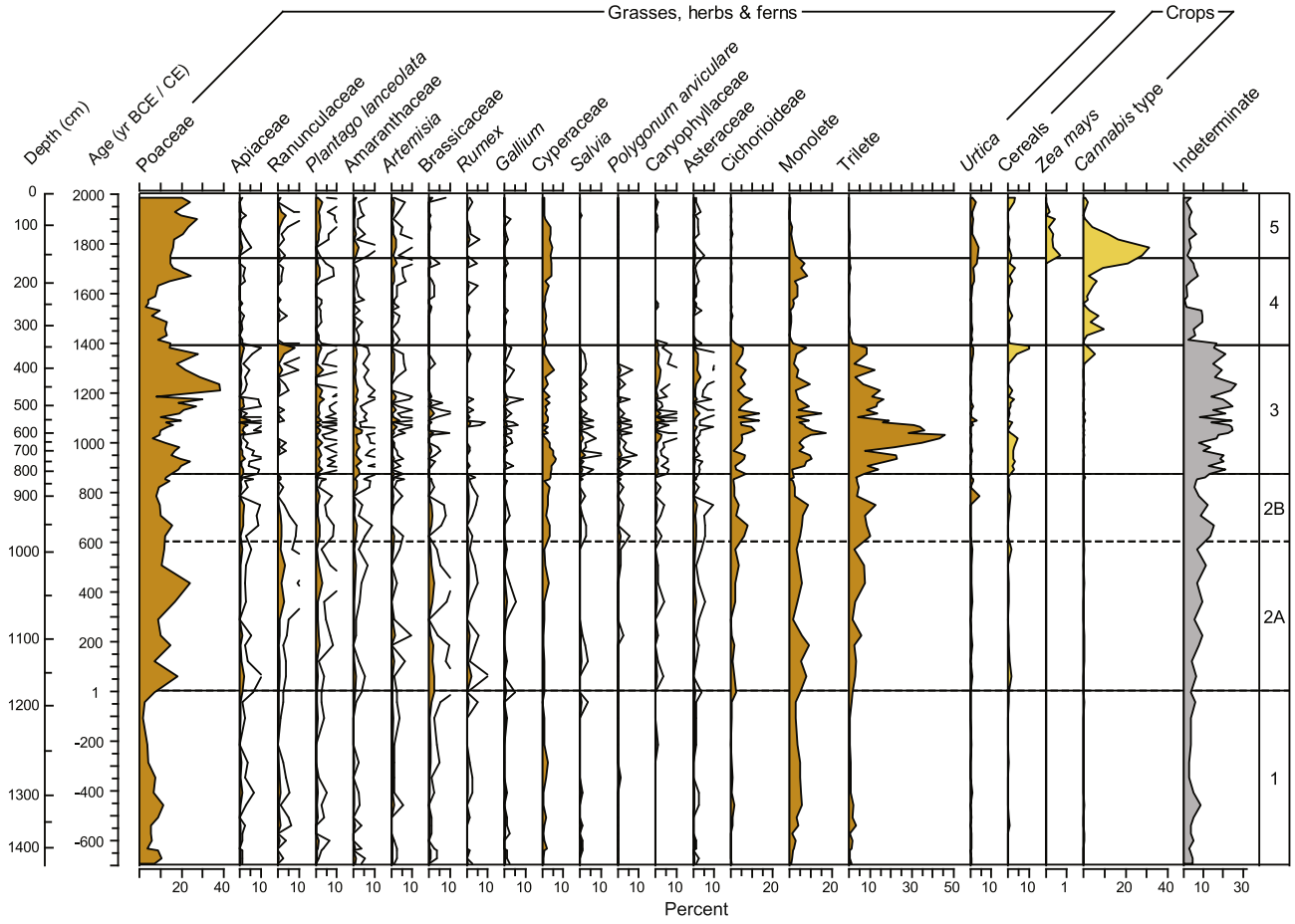

Fig. 12. Selected pollen taxa of herbs, crop plants and indeterminate pollen. Unfilled lines represent 5X exaggeration.

none of the other elements. The organic matter content is the highest throughout the core, following trends in both Ca and Sr.

4.3.4. Late modern to Contemporary interval 0–140 cm, Age: 1740–2000

This interval is composed of mottled and homogeneous to discontinuously laminated gray–black marl. The gray color appears to be related to carbonate content, with the lighter bands showing a higher percentage of carbonate grains. Diatoms are common as is aquatic organic matter. The carbonate fraction is more heterogeneous than lower intervals, and is composed of a mix of calcite rhombohedra, detrital allochems, *Phacodus*, and subordinate amounts of dendritic grains. There is a clay-sized siliclastic component, containing small amounts of fine (2–5 μm) silt grains.

4.4. Pollen, non-pollen palynomorphs and charcoal

We identified ninety different pollen types, nine non-pollen palynomorphs and eleven algae types. Pollen taxa with percentages consistently >1% are presented for trees (Fig. 11) and herbs (Fig. 12) and for the most abundant aquatic pollen, algae, and non-pollen palynomorphs (Fig. 13). Dominant taxa and percentages are summarized in Table 3.

Five pollen zones were interpreted from the dendrogram. Zone 1 (1438–1145 cm; 700 BCE to 1 CE) includes the Archaic, pre-Roman and Roman republican periods (Coccia et al., 1992). Zone 2 has been divided into two subzones; Zone 2A (2A, 1145–970 cm; 1 CE to 600 CE) corresponds to the Roman Imperial period through Late Antique period, and Zone 2B (970–800 cm; 600 to 870 CE) corresponds to the Early Medieval period. Zone 3 (800–335 cm; 870 to 1390 CE), corresponds to Medieval through Late Medieval time, Zone 4 (335–140 cm 1390 to 1730 CE) corresponds to the Early Modern and Modern periods, and Zone 5 (140–0 cm; 1730 CE to present) corresponds to the late Modern through Contemporary periods.

4.5. Interpretation of major phases of environmental change

There is a strong coupling between sedimentological and palynological shifts indicating that the factors affecting the lake's depositional environment were also at work affecting the plant cover in the surrounding landscape. The resolution of our age model is centennial to sub-centennial and allows us to identify the major shifts in environmental change to compare with the rich collection of archeological and archival evidence and independent climatic reconstructions. The record allows for recognition of distinct periods or phases within the last 2700 years. Here we discuss the seven most important environmental phases in a historical context and the potential climatic and human causes that may have caused those changes.

4.5.1. Pre-Roman: a climate driven system (700–300 BCE)

Environmental change during the pre-Roman period appears to be largely a response to climate rather than human activity. The

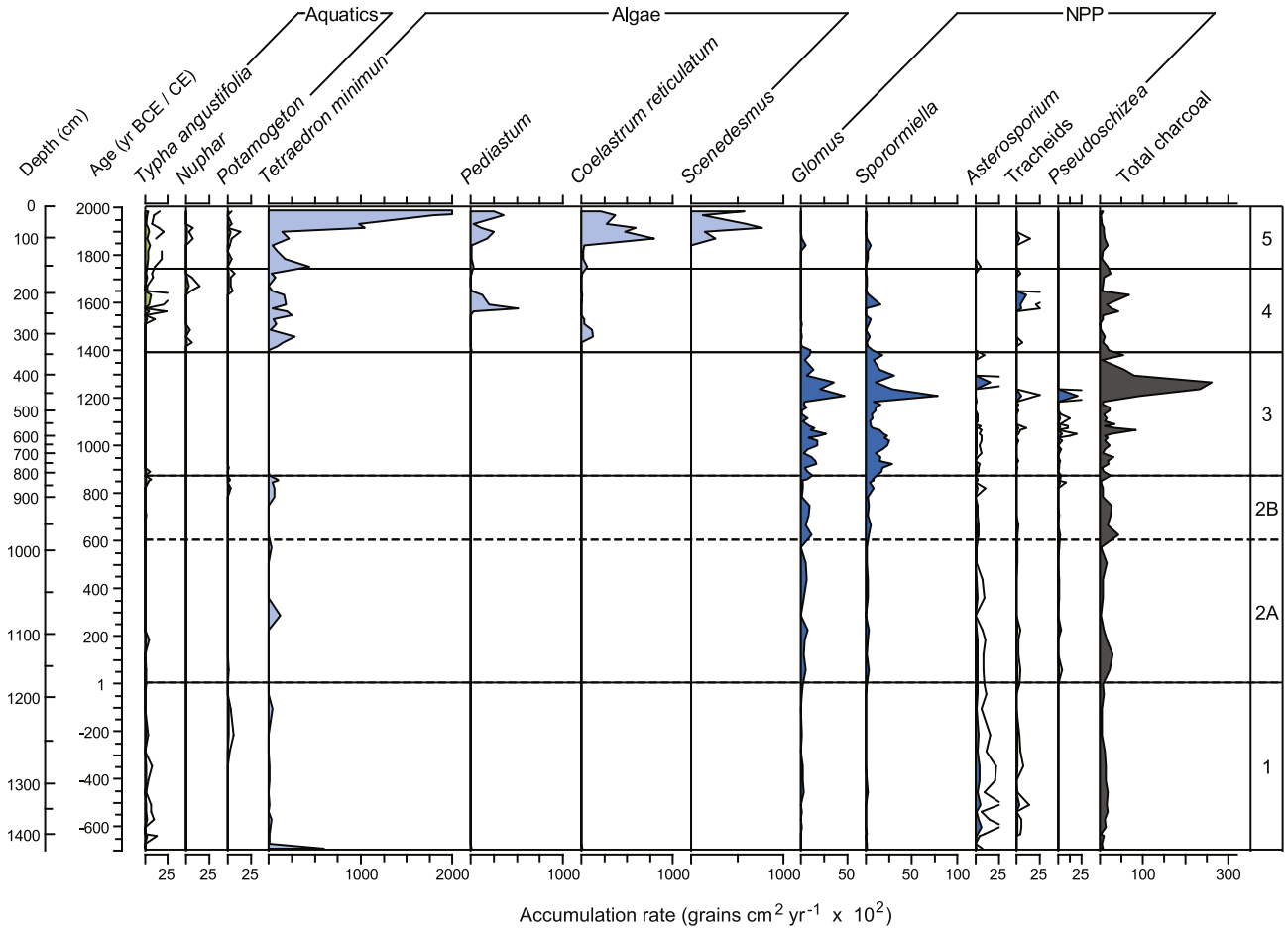

Fig. 13. Selected aquatic pollen, algae, non-pollen palynomorphs and charcoal. Units for charcoal are accumulation rate of number of pieces. Unfilled lines represent 5X exaggeration.

climate was cool and wet at the beginning of our record. The Calderone glacier, 50 km to the east in the Gran Sasso d'Italia mountain group, advanced between 900 and 750 BCE and periglacial soils are found in the Apennines during the same period (Giraudi, 2005; Giraudi et al., 2011). Archaeological excavations and surveys from near Lago Lungo reveal small settlements along the 375 m contour, suggesting habitation in a generally marshy environment around small lakes (Coccia et al., 1995). The Sabini, who inhabited the region, were an advanced culture and primarily exploited the land for pastoralism with little evidence of forest modification (Cifani, 2003). The literary tradition reports that in the Rieti Basin the cults of Vacuna and Hercules played an important role, the first as the deity of water and woods and the latter the god of springs and cattle (Alvino and Leggio, 2006; Camerieri, 2011).

There was a well-developed floodplain forest (*Alnus glutinosa* and *Fraxinus excelsior*) probably covering much of the basin floor and lakeshore and a rich mesophyllous forest (*Fagus*, deciduous and evergreen *Quercus*, *Ulmus*, *C. betulus*, *Acer*, and *Corylus*) on the uplands (Fig. 14). The abundance of *Fagus* pollen, and the presence of *Asterosporium*, a spore associated with *Fagus*, suggests that beech forests grew on the lower mountain slopes well below 1000 m, while today they are restricted above 900–1000 m (Piovesan et al., 2005).The mix of tree species as well as monolete and trilete ferns (e.g. *Osmundo-Alnion* and *Alno-Ulmion* alliances; Cutini et al., 2010) supports an interpretation of a minimally impacted forest (Russo Ermolli et al., 2014). This widespread mixed floodplain mesophyllous forest confirms that the landscape ecology of Central Italy was less affected by the Mid Holocene 'mediterraneanization' than other southern regions of the Mediterranean basin (Sadori et al., 2011).

The maximum highstand of *Lacus Velinus*, determined by geomorphic and archeological evidence (Ferreli et al., 1992), is reported to have occurred in the Iron Age (beginning ~850 BCE). The lake environment was a hydrologically open hard-water system (Ferreli et al., 1990) deep enough to support aquatic phytoplankton (i.e. cyclotelloid diatoms). Carbonate content and Ca relative abundance show a gradual decline in Lago Lungo from 700 to 400 BCE. The sediment accumulation rate during this period remains low, indicating that the decrease in carbonate is not due to dilution by clastic input. Instead, the carbonate trend reflects a change in lake chemistry affecting carbonate saturation and precipitation. The *Lacus Velinus* highstand reached an elevation of 375 m a.s.l., then dropped to ~372 m a.s.l. during pre-Roman time (pre 270 BCE), prior to any human modifications to the basin (Ferreli et al., 1990). The coincidence of a larger deeper lake in ~850 BCE, receding during pre-Roman times from its highstand supports the role of the water balance in affecting the observed carbonate trend. The gradual decline in carbonate content may reflect climatically-driven changes in lake hydrochemistry, although the specific drivers affecting carbonate deposition in this system need more investigation.

4.5.2. Roman Republican: initial manipulation of the drainage system (300–1 BCE)

About 270 BCE, the Romans are purported to have created *Cava Curiana*, a drainage canal cut through the travertine sill at the

Table 3
Description of key pollen taxa, non-pollen palynomorphs, algae, and charcoal results, summarized by pollen zonation. Percentages and accumulation rates are averages for the zone unless indicated otherwise.

Zone	Key taxa	Description of pollen, non-pollen palynomorphs, algae, and charcoal
Zone 5 140–0 cm 1740–2000 CE Late Modern & Contemporary	Poaceae *Quercus* (decid.) TC (*Juniperus*) *Ostrya* *Olea*	Modern landscape established. Poaceae (22% is the most common single pollen type and herbs (10.3%) have increased. Tree pollen (60.2%) is dominated by deciduous *Quercus* (19.7%), *Juniperus* (13.3%) and *Ostrya* (9.2%) with minor amounts of *Fagus*, *Fraxiunus ornus* and *Corylus* (each <1.5%). *Alnus* (1.5%) is nearly absent. *Olea* (3.8%) is important and shrubs (*Phillyrea* 2.9%) are now more abundant. Total pollen accumulation rate is 54,800 grains cm^{-2} yr^{-1}.
Zone 4 335–140 cm 1390–1740 CE Modern	*Quercus* (decid.) Poaceae *Alnus* *Ostrya* *Fagus* *Juglans* *Olea* TC (*Juniperus*)	Abrupt return to a forest phase. Percentage of tree pollen (73.0%) nearly as high as pre-Roman, although *Quercus* (30.2%) now much more common than other taxa; *Alnus* 10.8%), *Ostrya* (9.4%), *Fagus* 3.9%, *Ulmus*, *Fraxinus ornus*, *Corylus* and *Carpinus betulus* (each <1.6%). Tree crops emerge; *Olea* (1.4%) and *Juglans* (1.8%). Poaceae (11.9% and herbs (7.2%) decrease, ferns (2.1%) nearly disappear. TC (*Juniperus*) increases to 10.0% at 134 cm and *Cannabis* type peaks at 31.4%. Highest pollen accumulation rate (137,500 grains cm^{-2} yr^{-1}).
Zone 3 800–335 cm 870–1390 CE Medieval	Trilete/Monolete Poaceae *Quercus* (decid.) Cichorioideae Cereals *Sporormiella* *Glomus*	Abrupt transition to a deforested phase. Pollen of Poaceae (19.1%), herbs (21.0%) and fern (24.2%) more abundant than trees (31.7%). Trilete ferns average 17.7% and reach 55.7%. Cereals increase (1.6%) and associated weeds of cultivated land increase; Cichorioideae (6.2%), *Plantago*, Amaranthaceae, Asteraceae, Caryophyllaceae and Apiaceae (all >1%). *Sporormiella* (1130 grains cm^{-2} yr^{-1}) and *Glomus* (780 grains cm^{-2} yr^{-1}) increase. Charcoal (1380 grains cm^{-2} yr^{-1}) remains high. *Quercus* (13.6%) and *Alnus* (4.1%) decrease dramatically. Total pollen accumulation rate at lowest level (9800 grains cm^{-2} yr^{-1}).
Zone 2B 970–800 cm 870–600 CE Early Medieval	*Quercus* (decid.) *Alnus* *Ostrya* *Fagus* Poaceae Trilete/Monolete *Glomus*	Total forest pollen remains stable (60.5%) but diversity decreases. Poaceae (11.6%), herbs (15.6%) and total ferns (10.4%) also change little, but trilete ferns increase. Deciduous *Quercus* (20.9%), *Alnus* (13.4%) and *Salix* (2.0%) increase but all other tree taxa decline; *Ostrya* (7.3%), *Fagus* 4.5%), *Corylus* (2.6%), *Carpinus betulus* (<1%). *Glomus* (500 grains cm^{-2} yr^{-1}) and charcoal (1325 grains cm^{-2} yr^{-1}) both increase. Total pollen accumulation rate decreases (14,800 grains cm^{-2} yr^{-1}).
Zone 2A 1145–970 cm 1–600 CE Roman imperial and Late Antique	*Ostrya* *Alnus* *Quercus* (decid.) *Fagus* *Corylus* *Carpinus betulus* Poaceae Trilete/Monolete *Glomus*	Forest taxa, particularly *Alnus*, decrease but remain dominant (63.1%) and grasses (12.9%), herbs (12.7%) %) and ferns (9.1%) increase. Main tree pollen types are *Ostrya* (12.3%), *Alnus* (12.0%), deciduous *Quercus* (11.5%), *Fagus* (11.3%), *Corylus* (3.6%) and *Carpinus betulus* (2.1%). Herbs typical of disturbance begin to increase, including Cichorioideae (1.8%), Brassicaceae (1.5%), Ranunculaceae (1.4%) and *Plantago* (1.0%). Cereals (0.6%) increase and are consistently present. *Glomus*, an indicator of erosion, increases (380 grains cm^{-2} yr^{-1}) and charcoal reaches a peak (900 grains cm^{-2} yr^{-1}) in the 1st to 2nd centuries.
Zone 1 1438–1145 cm 700 BCE–1 CE Archaic, Pre-Roman & Roman Republic	*Alnus* *Quercus* (decid.) *Ostrya* *Fagus* *Carpinus betulus* *Asterosporium*	Forest phase dominated by tree pollen (81.3%). Herbs (5.9%), Poaceae (6.2%) and ferns (4.4%) are a small component of the pollen. Tree pollen is diverse composed of *Alnus* (21.2%), deciduous *Quercus* (18%), *Ostrya* (15.3%) and *Fagus* (8.6%) with small quantities of *Corylus* (3.3%), *Carpinus betulus* (3.2%), *Ulmus* (1.6%) and *Fraxinus excelsior* (1.3%). *Asterosporium* is at a maximum (260 grains cm^{-2} yr^{-1}). Total pollen accumulation rate is high (55,000 grains cm^{-2} yr^{-1})

location of the Marmore Falls to facilitate drainage and reclamation of the basin (Leggio and Serva, 1991). There is a magnetic susceptibility spike at ~300 BCE as well as an inflection point in many of the geochemical curves, including carbonate, TI and S, which may be associated with the channel cutting. The sediment remains dark gray to black with anoxic sulfides similar to the Pre-Roman core interval, and no discernible sedimentological change accompanies the magnetic susceptibility spike. However, if channel cutting served to lower Lago Lungo and temporarily isolate it from the larger lake system, then the subtle increases in the S signal seen above the magnetic susceptibility spike may reflect a more isolated stagnant lake with slightly more sulfidic mineralization. The steady decline in *Alnus* pollen beginning ~200 BCE (Fig. 14) supports an interpretation of a lowered water table; however, large areas of the valley must have remained wet given the continued persistence of *Alnus*. The decline in *Alnus* was permanent, indicating that after this change the basin never again reached the same extent of flooded forest. Pliny the Elder (*Naturalis historia* 3, 109) described the Rieti basin as covered by dense forest and beyond the change in *Alnus*, there is no evidence for forest degradation (Fig. 14).

Alnus requires standing water, and a reduction in *Alnus* suggests a reduction in wetland area in the valley. This interpretation supports the argument that the Romans first drained the Rieti Basin in the first quarter of the 3rd century BCE, as recorded by historians (Sisani, 2009). This reclamation work appears to have been sufficiently successful to have lowered the water table enough to reduce the flooded forests. The Roman water works do not appear to have changed land use practices. Archeological surveys indicate that local settlements were consolidated (Coccia et al., 1995) but in the 1st century BCE Varro emphasized the importance of sheep pasturing (Varr. 2.2.9) and the geographer Strabo described the Rieti valley as a place of domestic livestock, mules particularly (Strab. 5.3.1). The increase in disturbance taxa during this period supports an interpretation of increased pasturage.

4.5.3. Imperial Roman through Late Antique: intensification of land use (1–600 CE)

Climatically, the period from 1 to 200 CE is considered part of the Roman Optimum, with exceptional climate stability and favorable conditions that coincide with the rise of Imperial Rome

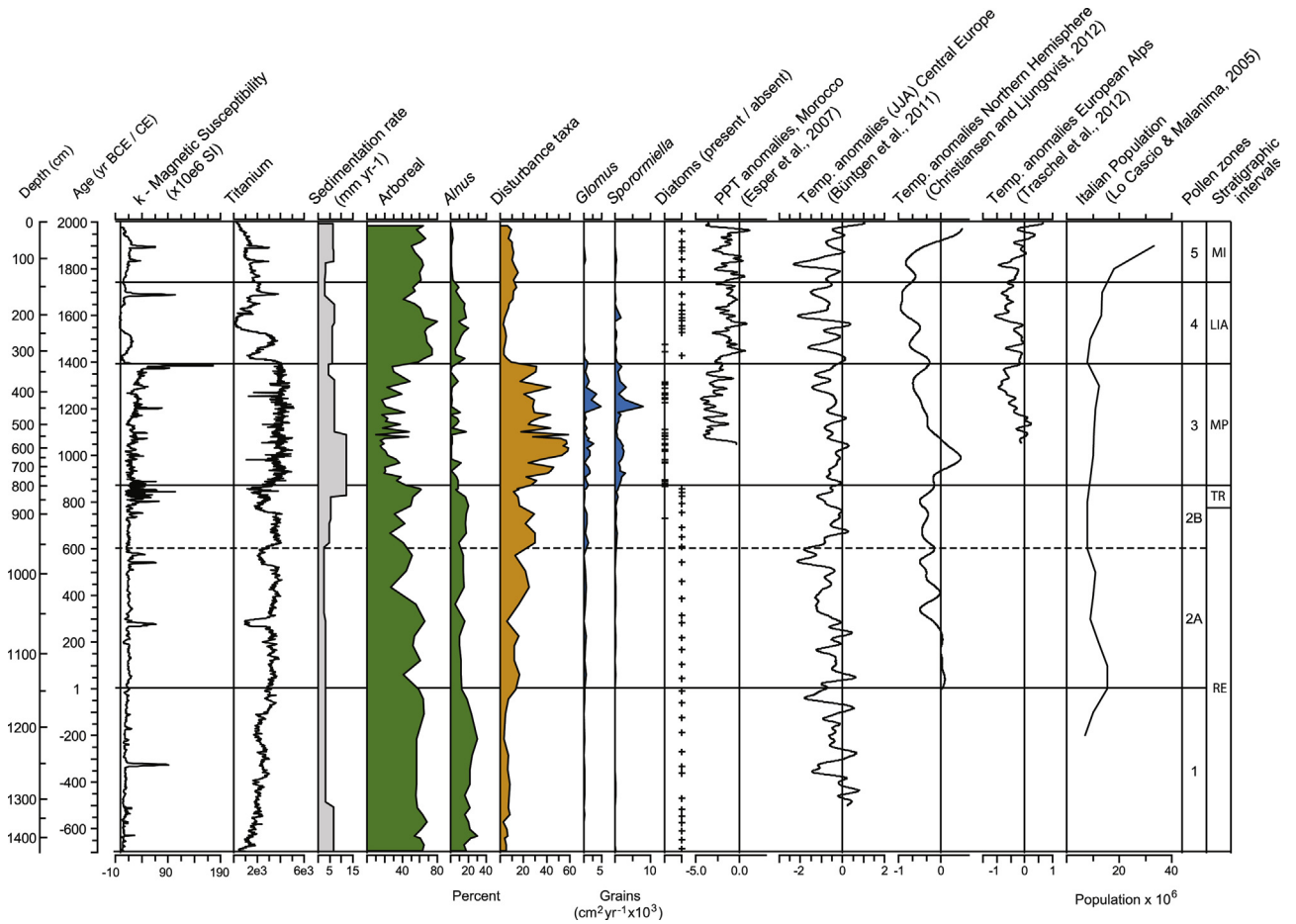

Fig. 14. Summary diagram with selected data. Arboreal pollen includes all tree taxa presented in Fig. 11 except *Alnus*. Disturbance taxa include all herbs plus trilete ferns shown in Fig. 12. Diatoms were identified from smear slide analysis. Stratigraphic intervals follow Fig. 10.

(McCormick et al., 2012). Reconstructed temperatures during this period were mild (Fig. 14), similar to the first half of the 20th century (Christiansen and Ljungqvist, 2012; northern hemisphere extratropical 2000 temperature reconstruction – ftp://ftp.ncdc.noaa.gov/pub/data/paleo/contributions_by_author/christiansen2012/christiansen2012.txt URL and data accessed). What is particularly striking is that while the population of Rome expanded to more than one million (Lo Cascio and Malanima, 2005) there is no evidence for intensive exploitation of the Rieti Basin through land clearance or deforestation. Forests declined during the Imperial period in relation to the Republican period (66% vs. 81% total AP respectively; Table 3, Fig. 14), though the extent of degradation appears limited. The impact on the forest shows alternating phases of more pressure (1st and 4th century) or less 3rd century (see also Russo Ermolli et al., 2014) consistent with the demographic and socio-economic trends of Rome (Leggio, 2000; Costambeys, 2009).

Around 1 CE there is an abrupt increase in disturbance species (e.g. *Rumex*, Brassicaceae, Cichorioideae, Apiaceae, and trilete spores) although a diverse flooded forest assemblage persisted. Pollen of cereals are present, but not abundant (Fig. 12) and *Sporormiella*, an indicator of domesticated livestock, is consistently present. Archeological evidence of settlement is restricted to the alluvial fans and low hill-slopes above the valley floor, concentrated between 380 and 480 m with no evidence of large settlements above 600 m (Coccia et al., 1995). The main nucleated settlement was Reate (Cifani, 2003) and the economy was probably oriented towards pastoralism and trade with the nearby Apennine communities. We infer that the basin was partially cleared for pasture but remained marshy and that livestock grazing was more important than agriculture, although even pasturage may not have been intensive.

A number of other pollen reconstructions from the Italian peninsula have also found only limited evidence of deforestation during the Roman Imperial period, including sites near Naples (Russo Ermolli and di Pasquale, 2002), Colli Euganei west of Venice (Kaltenrieder et al., 2010), Calabria (Joannin et al., 2012), Abruzzo (Branch and Marini, 2014) and near Ostia, the ancient port for Rome (Di Rita et al., 2010; Sadori et al., 2011). Our findings contrast with arguments for extensive forest clearing and burning in the vicinity of Rome (e.g. McNeil, 1992; Hughes, 2011) and support the argument that deforestation was localized and degradation limited (Grove and Rackham, 2001).

The Roman Empire supported a complex trade network and one possible reason for the lack of exploitation of the Rieti Basin may have been the 'globalization' of production of Imperial Rome. Rieti was interconnected with Rome and likely benefited from external resources, potentially reducing pressure on local resources (Champion, 1995). Local sites, such as Rieti, would not have been sufficient to support the large urban population of Rome and may have been spared from environmental degradation while distant regions were exploited. Egypt appears to have enjoyed exceptionally favorable conditions between 1 and 200 CE (McCormick et al., 2012) and food production and transport may have been more efficient from such distant locations as opposed to local sites with limited agricultural capacity and barriers to transport. Rieti was on

the Via Salaria, one of the most important trans-Apennine roads between Rome and the Adriatic Sea (Coccia et al., 1992), but the Marmore Falls prevent easy access by water to the Tiber River making it difficult to ship bulky resources (e.g. wheat, charcoal) to Rome. Another possibility is that, in order to prevent deforestation and soil erosion and to mitigate Tiber flooding in the area of *Lacus Velinus*, the forests were provided some level of protection as sacred woods, following the Sabini cult of Vacuna, identified as Vittoria or Diana by the Romans (Coccia et al., 1992; Alvino and Leggio, 2006).

Between 400 and 600 CE, during the Late Antique period, sometimes referred to as the Migration Period, we see a further degradation of the forest with a decline in *Ostrya* and increase in grassland (Poaceae), indicating more intensive coppicing of forests and possibly an intensification of local resource extraction. The Late Antique or Migration Period (400–600 CE), a time with cooler than average temperatures and general disruption following the Roman Empire (Büntgen et al., 2011; Christiansen and Ljungqvist, 2012), is sometimes identified as a period of climatic instability which may have contributed to cultural upheaval (McCormick et al., 2012). In Rieti, there are few indications of upheaval, however trade networks appear to have been disrupted requiring greater reliance on local products. With the fall of Rome, the Ostrogoths ruled Rieti between 400 and 570 CE and maintained the Roman system of governance (Leggio, 1989). Archaeological data support the presence of a thriving community (Coccia et al., 1995) though limited ceramics from this period indicate a potential breakdown in the trade system (Coccia et al., 1992). A decline in *Ostrya* and increase in disturbance taxa suggest possibly more intensive coppicing of forests and an intensification of local resource extraction, with less reliance on traded goods.

4.5.4. Early medieval: intensification of forest disturbance and sedimentation (600–900 CE)

This phase represents a transition period with a complex series of changes in the vegetation, sedimentary, magnetic and geochemical proxies. Between 600 and 735 CE temperatures in the northern hemisphere remained cooler than average (Christiansen and Ljungqvist, 2012) though in central Europe, climate became milder, with warming temperatures and an increase in precipitation (Büntgen et al., 2011). At our site, loss of forest biodiversity began ~600 CE, particularly the softer hardwoods (*Fagus*, *Tilia*, *Ulmus*, *Acer*, and *F. excelsior*) (Zone 2B, Fig. 11) and there was an increase in disturbance taxa (Fig. 12) and erosion (*Glomus*, Fig. 13). High percentages of *Alnus* indicate that the valley floor remained marshy, suggesting that human impacts were concentrated on the hill slopes.

A cool to mild climate should not have resulted in loss of forest biodiversity and we suggest that this environmental shift resulted from a change in the governing authority and associated changes in land use. The Lombards gained control of Rieti around 590 CE (Naspi, 2010). There are few written documents for this period, but Rieti has been described as changing from a city of stone to a city of wood (Leggio, 2000) and between ~600 and 800 CE, the softer desirable hardwoods appear to have been selectively removed initiating the decline in forest biodiversity (Fig. 11). In addition, the Farfa Monastery of the Benedictine order, established in the end of the 6th century in the Sabini Mountains (Fig. 1), became increasingly important in the 8th century. The monks were responsible for managing large areas of the landscape, including the Rieti Basin (Leggio, 1994) and forest cutting was widespread (Leggio and Serva, 1991).

From ~735 CE (900 cm depth) until ~870 CE (800 cm depth) the forest recovers somewhat, with an increase in *Quercus* and *Ostrya*, although there is no increase in the soft hardwoods. Disturbance indicators decrease, Ti decreases, carbonate and Ca increase, and MS is high and variable. Written sources describe an increase in flooded area, expansion of Lago Lungo (*lacus Totoni*) and Lago di Ripasottile (*lago Maggiore*) and the formation of many *lamae* (little lakes) (Leggio, 1994, 1998). This would appear to be a climatic impact, rather than a human induced change, though dominance of *Quercus* and *Ostrya* in the overstory suggests an actively coppiced forest.

4.5.5. Medieval through Late Medieval: peak deforestation and sedimentation (900–1390 CE)

The most extensive degradation of the environment occurred during the Medieval Period (~870–1390 CE) when forest cover was greatly reduced and herbs and ferns increased (Fig. 14). Temperatures in the northern hemisphere began warming after 900 CE with a well-defined peak between 950 and 1050 CE (Fig. 14) and a maximum temperature anomaly of 0.6 °C (Christiansen and Ljungqvist, 2012). Climate reconstructions from the central eastern Alps (Büntgen et al., 2011) and central Italy (Guiot and Corona, 2010) show elevated temperature from 700 to 1250 CE with a thermal maximum of 0.3 °C between 1053 and 1171 CE (Trachsel et al., 2012). A precipitation reconstruction (Palmer Drought Severity Index – PDSI) using *Cedrus atlantica* (Endl. Carrière) from Morocco (Esper et al., 2007; Trouet et al., 2009) shows that the period from 1050 to 1400 CE was anomalously dry across the western Mediterranean (Fig. 14). The initiation of forest cutting throughout the Rieti Basin coincides with the period of warmest temperatures, and climate change appears to have been a strong catalyst leading to environmental degradation; however socioeconomic changes are also important during this period.

Sediment accumulation rates reach their highest levels by 900 CE. The high percentages of indeterminate pollen (Fig. 12) as well as Cichorioideae, a taxon commonly found on disturbed sites with pollen particularly resistant to degradation (Bottema, 1975), support an interpretation of high erosion and increased bare soil. Cichorioideae have been demonstrated to be good indicators of open landscapes dominated by pastures and cultivated fields (Florenzano et al., 2015). Some of the indeterminate pollen are likely degraded tree taxa, could suggest that the level of deforestation may not have been as high as the pollen diagram indicates; however there is no reason to believe that the percentage of indeterminate pollen are skewed towards tree types since many herbaceous taxa are equally subject to degradation. Fern spores (trilete) are very high between 925 and 1075 CE. Ferns require mineral soil for regeneration, further supporting an interpretation that large areas with thin soils must have been present and loss of tree cover must have been widespread. The elemental proxy for erosion, the detrital element Ti, remains high throughout the MP, supporting the claim that deforestation and agricultural land use peaked during this time. Sediments throughout this phase are varicolored silty and clayey bands (Fig. 3) indicative of episodic sedimentation and potentially greater fluvial influence. The very high sediment accumulation rates begin to decline after 1100 CE.

Written and archeological evidence support the hypothesis for a large increase in population, leading to saturation of the lower elevation sites for agriculture, and a push to exploit higher elevations. During the Medieval period, settlements were constructed at elevations above 1000 m (Coccia et al., 1992). Terraced walls related to farming were found between 700 and 1000 m (Coccia et al., 1995) and active deforestation and a series of 'hospitals' for tending to farm workers have been documented at 1400 m (Naspi, 2010). It also seems reasonable to conclude that warmer temperatures allowed farming and grazing to be successful at higher elevations. As population grew and settlement expanded upslope, farmers likely pushed the limits of what local resources were

capable of supporting. Introduction of the heavy plough, horse collar and harrow were technological innovations that may have partially offset the limits of local production by permitting a more intensive agriculture (Sereni, 1973).

Documents record an increase in deaths due to malaria (Bruce-Chwatt and de Zulueta, 1980; Sabbatani, 2005) which may have also contributed to building settlements at higher elevation (Leggio, 1994). Settlement was not dispersed, but largely concentrated in fortified settlements or castles (*incastellamento*) for security. More than forty settlements in the Rieti Basin are first mentioned in the Farfa monastery documents in the period between 1050 and 1200 CE, of which fifteen of these hill towns are still occupied (Coccia et al., 1992). Dispersed settlements did not completely disappear, but the broad pattern was one of the population concentrated into fortified settlements in defensible locations governed by powerful and wealthy lords (Leggio, personal communication). A sharp decline and intermittent absence of *Alnus* from the record indicates that the valley must have also been heavily managed and utilized for cereal production. Only through constant maintenance of the drainage system was it possible to prevent the basin from becoming marshland (Coccia et al., 1992). This maintenance was probably aided by a drier than normal climate (Fig. 14) and large available labor force. A possible explanation for the new phase of exploitation of the valley is that the slopes were not sufficient to maintain the needs of the increasing population (Naspi, 2010).

Following the MWP thermal maximum, the initial cooling of the LIA began, reaching a temperature anomaly of −0.8 °C about 1310 CE (Fig. 14; Büntgen et al., 2011; Christiansen and Ljungqvist, 2012; Trachsel et al., 2012). The black plague of 1347 CE, and subsequent famines and plagues resulted in a local population decline of >50% by 1400 CE (Leggio, 1989). Cooler than average temperatures between 1350 and 1390 CE appear to have been a catalyst leading to collapse of the local land management system. As high elevation settlements were abandoned (Leggio, 1995b; Naspi, 2010) disturbance species decreased, and forest taxa and *Alnus* begin to steadily increase (Fig. 14).

4.5.6. Little Ice Age: rapid reforestation and reduced sedimentation (1390–1700 CE)

A combination of climatic change, plague, earthquakes and political instability led to a collapse of the local system by the early 15th century. Precipitation increased and temperatures remained cool (Büntgen et al., 2011; Christiansen and Ljungqvist, 2012). By ~1390 CE, the PDSI reconstruction from Morocco records anomalously wet conditions (Fig. 14), with peak wetness in the 15th and 16th centuries (Esper et al., 2007). Records of major floods on the Tiber River through Rome began an upswing in the 14th century and reached a maximum in the 15th century with a total of seventeen major floods, an average of one every 6 years (Bersani and Bencivenga, 2001; Giraudi, 2012). In contrast, only three major floods were recorded in the 13th century. San Matteo church documents and the 1445 CE Rieti cadastral survey indicate that lakes in the basin reached their maximum extent during this period (Leggio, 2007).

The rock magnetic parameters (Fig. 5) indicate a significant event at the very end of the Medieval interval (337 cm depth, ~1380 CE) followed immediately by changes in the geochemical data (Fig. 10) and representing a permanent change in the sedimentary dynamics in the lake. All clastic proxies (κ, Ti, and smear-slide petrography) dropped to zero at 335 cm depth. Such a change required an abrupt adjustment to the sedimentary environment, cutting off all access of siliciclastic input. This shift coincided with a series of physical influences on the environment (strong earthquakes in central Italy (Galli and Nasso, 2009) and increased precipitation) as well as socioeconomic influences (depopulation following the Black Plague, local political instability). Historical documents of the second half of the 14th century report difficulties in managing the drainage system of the basin and consequent famine (Leggio and Serva, 1991). The geochemistry is very distinct with large peaks in Sr, S and Ca (Fig. 10) that are indicative of changes in water chemistry and potentially a rearrangement of source waters to include a more SO_4-rich source.

Increasingly cooler temperatures pushed people out of the highest elevation settlements, resulting in widespread land abandonment (Leggio, 1995b; Naspi, 2010) and rapid recovery of forests. Recurring plagues through the first half of the 16th century (Barbiera and Dalla-Zuanna, 2009; Tozzi, 2009; Alfani, 2010) reduced the Italian population to its lowest level in Medieval time (Fig. 14) by the mid-15th century (Capasso and Malanima, 2007). The peak in percent arboreal pollen and pollen accumulation rate ~1600 CE coincides with the coolest temperatures during the LIA (Ladurie, 1971). This pattern of land abandonment and reforestation following demographic decline from the black plague, and deterioration of the climate has been documented repeatedly throughout Europe (van Hoof et al., 2006; Yeloff and van Geel, 2007; Fraser, 2011). While the reforested phase in many northern European sites lasted about a century, it lasted for two centuries in Italy. Political instability and the persistent presence of mercenary bands made it increasingly unsafe to pasture livestock far from settlements and hunting and fishing became increasingly important (Lorenzetti, 1989). By the mid-15th century, the meat of deer and wild boar was less expensive than that of domesticated animals and predators such as bears and wolves were present (Leggio, 1995a) providing evidence for return of a functioning forest ecosystem. This pattern of the increased importance of game over domesticated animals has been documented in France as well (Vecchio, 1974).

Despite extensive land clearing and erosion during the Medieval Period, forests quickly recovered during the Little Ice Age (Fig. 14), although forest biodiversity did not return to the level of the Roman and pre-Roman periods. One possible reason for the quick recovery may have been associated with the practice of coppicing, in which, although dramatically thinned, stems remain in the landscape and stem sprouts grow rapidly in the absence of repeated cutting. High percentages of *Alnus* indicate that the basin must have been flooded through much of this period. The lake expansion in the 15th century was so widespread in the basin that the 1445 CE cadaster reported thirty-eight small lakes (Leggio and Serva, 1991); moreover in the historical maps of 1500–1600 CE the flooded area is expanded, often reported as a single lake.

Tree crops, particularly *Olea* (olive) and *Juglans* (walnut), became more important after 1390 CE (Fig. 11). Around 1350 CE, a set of local regulations were codified governing the pruning and maintenance of tree crops (Caprioli, 2008). During Medieval time, olives as well as walnut were not important food crops in this interior area of the Sabina (Leggio, 1995b; Naspi, 2010) but after 1390 CE they increased in abundance and became a larger proportion of the diet. Following an initial increase in *Olea* pollen, there is a distinct decrease in abundance between ~1550 and 1650 CE, coincident with an intense cold period documented throughout central and southern Europe, with the coldest temperatures occurring in the late 16th and early 17th centuries (Ladurie, 1971; Trachsel et al., 2012; Moriondo et al., 2013). At least seven different years with olive-killing frosts were recorded in Provence, France between 1565 and 1600 CE (Ladurie, 1971). The Rieti basin is a marginal environment for olives and the decline in pollen is likely attributable to repeated killing frosts.

After 1600 CE *Alnus* pollen shows a continuous and permanent decline providing evidence for a lowering water table (Fig. 14)

despite steady or increased precipitation (Esper et al., 2007). Since the 13th century, many efforts had been made to construct new channels to remove water from the basin, including an unnamed channel in 1325 CE, *Cava Reatina* (1422 CE), *Cava Paolina* (1547 CE) and *Cava Gregoriana* (1575 CE). These efforts were largely unsuccessful until construction of *Cava Clementina* in 1601 CE (Lorenzetti, 1989; Leggio and Serva, 1991). Decline in *Alnus* after 1600 CE appears to be a response to human activity rather than climate.

4.5.7. Late Modern and Contemporary: modern forest with lake eutrophication (1700 CE to present)

By the 18th century, the vegetation structure was essentially modern. Drainage of the basin removed all flooded forest and agriculture included introduced crops such as *Z. mays* (Fig. 11). *Cannabis* type production peaked in the late 18th and early 19th centuries, with the very high pollen percentages likely associated with retting in pools adjacent to the lake (Celetti, 2007). The slopes remained forested but contained much less biodiversity than the original landscape, even though pollen percentages suggest that total forest cover is not significantly less now than during the pre-Roman period. The successional species *Juniperus communis* and *J. oxycedrus* are now an important forest constituent whereas for most of the record they were a minor component of the vegetation. The lakes appear to have become increasingly eutrophic with dramatic increases in diatoms, soft-bodied algae and calcareous algae towards the present (Fig. 13). The intensity of human impacts increased such that the human signal of environmental change is much stronger than the climate signal.

5. Conclusions

Our 2700 year paleoenvironmental reconstruction on the fringes of Rome records a complex interaction between climate and socioeconomic conditions as drivers of environmental change. The influence of Rome on the Rieti Basin during the Roman Republican Period seems to be modest. Despite the channel excavations that formed the falls at Marmore and drained the basin, our multi-proxy record indicates that the effects on both the aquatic ecosystem and landscape were minimal. During the Imperial Roman Period, a time of generally mild climate referred to as the Roman Optimum, there is no evidence for deforestation in the Rieti Basin and only limited impact on the environment, although Rome reached one million inhabitants. The Roman Empire supported a complex trade network that allowed importing resources from distant regions, similar to modern globalization. Rieti was interconnected with Rome and likely benefited from external resources, which reduced pressure on its local resources, resulting in preservation of the environment. With the fall of Rome, despite a cooler climatic period associated with an interval of general disruption in central Europe referred to as the Migration Period, the Ostrogoths filled the power vacuum in Rieti and generally maintained an environment similar to that which existed during the Roman period. Only with the arrival of the Lombards and establishment of local monasteries at the start of the Medieval Period (~600 CE) does deforestation become apparent, with clearing for agriculture and selective removal of desirable tree species for housing and manufacture. This period is manifested in a strong signal in the Lago Lungo record that transgresses all of the biological, geochemical, and sedimentological proxies.

The climatically optimal Medieval Warm Period appears to have been a catalyst for expanded land use and widespread environmental degradation. Local population was higher than during Roman time, placing greater pressure on local resources, but another possibly crucial difference was the lack of an interconnected trade network capable of supplementing local resources. As population grew and settlements expanded upslope, they likely pushed the limits of what local resources were capable of supporting. When a cooling trend began in the 13th century, the highest elevations began to be abandoned and the forests began to recover somewhat. By the late 14th century, plague devastated the local population. Persistent cooler and wetter climate led to wide scale land abandonment and rapid reestablishment of the forest and wetlands. Climate change, coinciding with earthquakes produced marked changes in the local sedimentological regime of Lago Lungo, including diversion of siliclastic input and altered lake hydrochemistry. The Medieval period in Rieti has a complex socioeconomic history, but the evidence supports the argument that the shift from warm and mild climate to cool and wet climate was an important catalyst in disrupting the community. This disruption lasted for nearly two centuries. By the 1600s, despite being one of the coldest periods of the LIA, improved methods in hydrologic works led to the eventual permanent draining of the basin and renewed agricultural expansion which has continued to today.

The detailed reconstruction of climatic and environmental changes from sedimentary records is dependent upon reliable dating of the sedimentary sequences. In the case of Lago Lungo interpretation of the ^{14}C dates is challenging; however the sediments are characterized by good paleomagnetic properties, with an almost single-component ChRM that can be easily isolated with stepwise AF demagnetization. The ChRM inclination and declination values oscillate around the mean values expected for the GAD field at the site, but the amplitude and the frequency of the variation are too high for geomagnetic secular variation. The paleomagnetic trends (ChRM inclination, declination and relative paleointensity) can be replicated at high-resolution between four distinct cores, ruling out disturbance as a cause for this variation. Regardless of the high-amplitude and high-frequency variation, when broadly smoothed the reconstructed paleomagnetic trends can be correlated to the reference curves from models of paleosecular variation (PSV) during the last 3000 years, as reconstructed from archeomagnetic data collected across Europe. Together with constraints coming from pollen and sediment analysis, the paleomagnetic trends allow the construction of a high-resolution age model and indicate that some changes observed in the pollen assemblage and in sedimentation in the Rieti basin can be associated to societal factors and others to climatic change. Paleomagnetism is a powerful tool for providing alternative age models for study sites with ^{14}C records that are difficult to interpret. The rich documentary record for the region provides an opportunity to further explore questions of environmental change in relation to societal versus climatic causes. Addressing some of these questions will require further refinement of our age model to reduce temporal uncertainty.

Contributions by authors

Mensing co-led the field coring, analyzed pollen, contributed to development of the age model and climate proxy framework, and oversaw the project; Tunno assisted in field coring and analyzed pollen and charcoal; Sagnotti and Florindo conducted all rock magnetism and paleomagnetism analyses and developed the PSV age model; Noble created the core description, conducted smear slide analysis and analyzed elemental chemistry; Archer analyzed elemental chemistry; Zimmerman conducted all radiocarbon analyses and helped develop the age model; Pavón-Carrasco helped develop the age model and associated error analysis; Cifani and Passigli conducted historical archival research (Section 3.7), contributed interpretation of historical documents, and specifically authored historical sections in paragraphs 4.5.1, 4.5.2; 4.5.3 by G. Cifani and paragraphs 4.5.4, 4.5.5, 4.5.6, 4.5.7 by S. Passigli;

Piovesan coordinated all Italian research components, co-led the field coring, interpreted pollen results in relation to local forest ecology, contributed to development of the age model and climate proxy framework and contributed to historical research. All co-authors contributed to writing the manuscript.

Acknowledgements

We are grateful to the many people who helped make this study possible, Microtephra analysis was performed by Paola Del Carlo, Antonella Bertagnini, Alessio di Roberto of INGV, Pisa, Italy. Cores were processed at LACORE, Minneapolis with assistance from Anders Noren, Christina Brady, Amy Mybro and Jessica Heck. Fig. 1 was created by Emanuele Ziaco. Funding was provided by the National Science Foundation (GSS-1228126) to Mensing and Noble, international travel awards and sabbatical leave from the University of Nevada, Reno to Mensing, the Sabina Universitas and Province of Rieti. We are grateful to Luigi Sandoletti for technical support, Giulia Sandoletti for laboratory assistance, Emanuele Presutti Saba, Emanuele Ziaco, and Gianluca Bonavigo for field and coring assistance, and DAFNE Università degli Studi della Tuscia for field transportation. Paolo Bellezza, Maurizio Sterpi at the Riserva Naturale dei Laghi Lungo e Ripasottile provided housing at the field site and boat access to Lago Lungo. Stefano Pizetti helped arrange housing in Viterbo for U.S. participants. Comments from an anonymous reviewer significantly improved the manuscript. This is LLNL-JRNL-665781.

References

Aimers, J., 2011. Drought and the Maya; the story of artefacts. Nature 479, 4–5.
Alfani, G., 2010. Pestilenze e 'crisi di sistema' in Italia tra XVI e XVII secolo. Perturbazioni di breve periodo o cause di declino economico? In: Cavaciocchi, S. (Ed.), Le interazioni fra economia e ambiente biologico nell'Europa preindustriale. Florence University Press, Florence.
Alvino, G., Leggio, T., 2006. Acque e culti salutari in Sabina, in Usus veneratioque fontium 2006.
Barbiera, I., Dalla-Zuanna, G., 2009. Population dynamics in Italy in the Middle Ages: new insights from Archaeological findings. Popul. Dev. Rev. 35, 367–389.
Berglund, B.E., 2003. Human impact and climate changes—synchronous events and a causal link? Quat. Int. 105, 7–12.
Bersani, P., Bencivenga, M., 2001. Le piene del Tevere a Roma dal V secolo a.C. all'anno 2000. Presidenza del Consiglio dei Ministri, Roma, p. 8.
Beug, H.J., 2004. In: Pfiel (Ed.), Leitfaden der Pollenbestimmung fur Mitteleuropa und angrenzende Geiete, p. 542. Munchen.
Blackmore, S., Steinmann, J.A.J., Hoen, P.P., Punt, W., 2003. The Northwest European Pollen Flora, 65. Betulaceae and Corylaceae. Rev. Palaeob. Palynol. 123, 71–98.
Bottema, S., 1975. The interpretation of pollen spectra from prehistoric settlements (with special attention to Liguliflorae). Palaeohistoria 57, 17–35.
Branch, N.P., Marini, N.A., 2014. Mid-Late Holocene environmental change and human activities in the northern Apennines, Italy. Quat. Int. 353, 34–51.
Brown, A.G., Hatton, J., Selby, K.A., Leng, M.J., Christie, N., 2013. Multiproxy study of Holocene environmental change and human activity in the Central Apennine Mountains, Italy. J. Quat. Sci. 28 (1), 71–82.
Bruce-Chwatt, L.J., de Zulueta, J., 1980. The Rise and Fall of Malaria in Europe. Oxford University Press, Oxford.
Büntgen, U., Teleg, W., Nicolussi, K., McCormick, M., Frank, D., Trouet, V., Kaplan, J.O., Herzing, F., Heussner, K.-U., Wanner, H., Luterbacher, J., Esper, J., 2011. 2500 years of European climate variability and human susceptibility. Science 311, 578–582.
Caciorgna, M.T., 1998. Popolamento e agricoltura: aspetti della politica territoriale del comune di Rieti nel Duecento. In: Grillotti di Giacomo, M.G., Moretti, L. (Eds.), I valori dell'agricoltura nel tempo e nello spazio, vol. I. Brigati, pp. 82–97.
Caciorgna, M.T., 2000. Confini e giurisdizioni tra Stato della Chiesa e Regno. In: Hubert, E. (Ed.), Une région frontalière au Moyen Âge. Les Vallées du Turano et du Salto entre Sabine et Abruzzes, Paris, pp. 307–326.
Calderini, G., Calderoni, G., Cavinato, G.P., Gliozzi, E., Paccara, P., 1998. The upper Quaternary sedimentary sequence at Rieti Basin (central Italy): a record of sedimentation response to climatic changes. Palaeogeogr. Palaeoclimatol. Palaeoecol. 140, 97–111.
Calderoni, G., Carrara, C., Ferreli, L., Follieri, M., Gliozzi, E., Magri, D., Narcisi, B., Parotto, M., Sadori, L., Serva, L., 1994. Palaeoenvironmental, palaeoclimatic and chronological interpretations of a late Quaternary sediment core from Piana di Rieti (central Apennines, Italy). Giorn. Geol. 3 (56/2), 43–72.
Camerieri, T.M., 2011. Transumanza e agro centuriato in alta Sabina, interferenze e soluzioni gromatiche. Lazio Sabina 7, 111–127.
Capasso, S., Malanima, P., 2007. Economy and population in Italy 1300–1913. Popol. Stor. 2, 15–40.
Caprioli, M., 2008. Lo statuto della città di Rieti: dal secolo XIV al secolo XVI. Istituto storico italiano per il Medio Evo.
Casella, L., Agrillo, E., Spada, F., 2009. Descrizione del patrimonio botanico e proposte di gestione della riserva naturale regionale Laghi Lungo e Ripasottile e della ZPS. In: La riserva naturale dei Laghi Lungo e Ripasottile, conoscenza e pianificazione, Rieti.
Cavinato, G., De Celles, P., 1999. Extensional basins in the tectonically bimodal central Apennines fold-thrus belt, Italy: response to corner flow above a subducting slab in retrograde motion. Geology 27 (10), 955–958.
Celetti, D., 2007. La canapa nella Repubblica veneta. In: Produzione nazionale e importazione in età moderna. Istituto veneto di Scienze, Lettere ed Arti, Venezia.
Champion, T., 1995. Centre and Periphery: Comparative Studies in Archaeology. Routledge, 264 pp.
Chester, P.I., Raine, J.I., 2001. Pollen and spore keys for Quaternary deposits in the northern Pindos Mountains, Greece. Grana 40 (6), 299–387.
Christiansen, B., Ljungqvist, F., 2012. The extra-tropical Northern Hemisphere temperature in the last two millenia: reconstructions of low-frequency variability. Clim. Past 8, 765–786.
Cifani, G., 2003. Storia di una frontiera. Dinamiche territoriali e gruppi etnici nella media valle tiberina dalla prima età del ferro alla conquista romana. Istituto Poligrafico e Zecca dello Stato, Roma.
Coccia, S., Mattingly, D.J., Beavitt, P., Elton, H., Foss, P., George, I., Hunt, C.O., Leggio, T., Patterson, H., Roberts, P., Brehm, T., Sudell, T., Sherratt, M., Morton, K., 1992. Settlement History, Environment and Human Exploitation of an Intermontane Basin in the Central Apennines: The Rieti Survey 1988–1991, Part I. In: Papers of the British School at Rome, vol. 60, pp. 213–289.
Coccia, S., Mattingly, D.J., Brehm, B., Elton, H., Foss, P., George, I., Leggio, T., Patterson, H., Roberts, P., Sudell, T., 1995. Settlement History, Environment and Human Exploitation of an Intermontane Basin in the Central Apennines: The Rieti Survey 1988–1991, Part II. Land-use patterns and Gazetteer. In: Papers of the British School at Rome, vol. 63, pp. 105–158.
Coombes, P.M.V., Chiverrell, R.C., Barber, K., 2009. A high-resolution pollen and geochemical analysis of late Holocene human impact and vegetation history in southern Cumbria, England. J. Quat. Sci. 24 (3), 224–236.
Cosentino, D., Cipollari, P., Marsili, P., Scrocca, D., 2010. Geology of the central Apennines: a regional reviewMarco Beltrando, Angelo Peccerillo, Massimo Mattei, Sandro Conticelli, and Carlo Doglioni, the Geology of Italy: Tectonics and Life along Plate Margins. J. Virt. Explor. Electron. Ed. ISSN: 1441-8142 vol. 36. http://dx.doi.org/10.3809/jvirtex.2010.00223 paper 12.
Costambeys, M., 2009. Settlement, taxation and the condition of the peasantry in Post-Roman Central Italy. J. Agrar. Chang. 9 (1), 92–119.
Covino, R., 1995. L'invenzione di una regione. In: L'Umbria dall'Ottocento a oggi. Quattroemme Editore, Perugia, p. 142.
Croudace, I.W., Rindby, A., Rothwell, R.G., 2006. ITRAX; description and evaluation of a new multi-function X-ray core scanner. Geol. Soc. Spec. Publ. 267, 51–63.
Cugny, C., Mazier, F., Galop, D., 2010. Modern and fossil non-pollen palynomorphs from the Basque mounatains (western Pyrenees, France): the use of coprophilous fungi to reconstruct pastoral activity. Veg. Hist. Archaeobot. 19, 391–408.
Cutini, M., Cancellieri, L., Cioffi, M.T., Licursi, C., 2010. Phytosociology and phytogeography of fragmented *Alnus glutinosa* forests in a Tyrrhenian district (Central Italy). Ecol. Mediterr. 36 (2), 56.
Dean Jr., W.E., 1974. Determination of carbonate and organic matter in calcareous sediments and sedimentary rocks by loss on ignition: comparison with other methods. J. Sed. Petrol. 44, 242–248.
De Felice, R., 1965. In: Aspetti e momenti della vita economica di Roma e del Lazio nei secoli XVIII e XIX. di storia e letteratura, vol. 13.
Dearing, J.A., Jones, R.T., Shen, J., Yang, X., Boyle, J.F., Foster, G.C., Crook, D.S., Elvin, M.J.D., 2008. Using multiple archives to understand past and present climate-human-environmental interaction: the lake Erhai catchment, Yunnan Province, China. J. Paleolimnol. 40, 3–31.
De Santis, A., Coarelli, F., 2009. In: Quasar (Ed.), Reate e l'Ager Reatinus: Vespasiano e la Sabina: dalle origini all'impero, p. 192. Roma.
Diamond, J., 2005. Collapse: How Societies Choose to Fail or Succeed. Viking, London, 575 pp.
Di Rita, F., Melis, R.T., 2013. The cultural landscape near the ancient city of Tharros (central West Sardinia): vegetation changes and human impact. J. Archaeol. Sci. 40 (12), 4271–4282.
Di Rita, F., Celant, A., Magri, D., 2010. Holocene environmental instability in the wetland north of the Tiber delta (Rome, Italy): sea-lake-man interactions. J. Paleolimnol. 44 (1), 51–67.
Di Rita, F., Magri, D., 2009. Holocene drought, deforestation, and evergreen vegetation development in the central Mediterranean: a 5500 year record from Lago Alimini Piccolo, Apulia, southeast Italy. Holocene 19, 295–306.
Dupré, T.E., 1939. Il lago Velino. In: Saggio storico-geografico, Consorzio di bonifica della Piana reatina nel decennale della legge Mussolini, Rieti.
Esper, J., Frank, D., Büntgen, U., Verstege, A., Luterbacher, J., Xoplaki, E., 2007. Long-term drought severity variations in Morocco. Geophys. Res. Lett. 34, L17702. http://dx.doi.org/10.1029/2007GL030844.
Faegri, K., Iversen, J., 1985. Textbook of Pollen Analysis, fourth ed. Hafner Press, New York.

Ferreli, L., Brunamonte, F., Filippi, G., Margheriti, L., Michetti, A.M., 1992. Studi Geologici Camerti, vol. Speciale 1, pp. 127–135.
Ferreli, L., Parotto, M., Serva, L., 1990. Evoluzione del reticolo idrographico nella Piana di Rieti degli ultimi 4000 anno. Mem. Soc. Geol. Ital. 45, 90–910.
Florenzano, A., Marignani, M., Rosati, L., Fascetti, S., Mercuri, A., 2015. Are Cichorieae an indicator of open pastures and pastoralism in current and past vegetation studies? Plant Biosyst. 149, 154–165.
Fraser, E.D.G., 2011. Can economic, land use and climatic stresses lead to famine, disease, warfare and death? Using Europe's calamitous 14th century as a parable for the modern age. Ecol. Econ. 70, 1269–1279. http://dx.doi.org/10.1016/j.ecolecon.2010.02.010.
Gallet, Y., Genevey, A., Le Go, M., 2002. Three millennia of directional variations of the Earth's magnetic field in western Europe as revealed by archaeological artefacts. Phys. Earth Planet. Int. 131, 81–89. http://dx.doi.org/10.1016/S0031-9201(02)00030-4.
Galli, A., 1840. Cenni economico-statistici sullo stato pontificio con appendice. Discorso sull'agro romano e sui mezzi di migliorarlo. Tipografia Camerale, Roma.
Galli, P., Naso, J., 2009. Unmasking the 1349 earthquake source (southern Italy): paleoseismological and archaeoseismological indications for the Aquae Iuliae fault. J. Struct. Geol. 31, 128–149.
Giaccio, B., Messina, P., Sposato, A., Volaggio, M., Zanchetta, G., Galadini, F., Gori, S., Santacroce, R., 2009. Tephra layers from Holocene lake sediment of the Sulmona Basin, central Italy: implications for volcanic activity in Peninsular Italy and tephrostratigraphy in the central Mediterranean area. Quat. Sci. Rev. 28, 2710–2733.
Giraudi, C., 2005. Late-Holocene alluvial events in the Central Apennines, Italy. Holocene 15 (5), 768–773.
Giraudi, C. The Holocene record of environmental changes in the 'Stagno di Maccarese' marsh (Tiber river delta, central Italy). Holocene 22 (12), 2012, 1461–1471.
Giraudi, C., Magny, M., Zanchetta, G., Drysdale, R.N., 2011. The Holocene climatic evolution of Mediterranean Italy: a review of the continental geological data. Holocene 21 (1), 105–115.
Grove, A.T., Rackham, O., 2001. The Nature of Mediterranean Europe: an Ecological History. Yale University Press, New Haven.
Guiot, J., Corona, C., 2010. Growing season temperatures in Europe and climate forcings over the past 1400 years. PLoS one 5 (4), e9972.
Haberzettl, T., Kück, B., Wulf, S., Anselmetti, F., Ariztegui, D., Corbella, H., Fey, M., Janssen, S., Lücke, A., Mayr, C., Ohlendorf, C., Schäbitz, F., Schleser, G., Wille, M., Zolitschka, B., 2008. Hydrological variability in southeastern Patagonia and explosive volcanic activity in the southern Andean Cordillera during Oxygen Isotope Stage 3 and the Holocene inferred from lake sediments of Laguna Potrok Aike, Argentina. Palaeogeogr. Palaeoclimatol. Palaeoecol 259, 213–229.
Haenssler, E., Nadeau, M., Vött, A., Unkel, I., 2013. Natural and human induced environmental changes preserved in a Holocene sediment sequence from the Etoliko Lagoon, Greece: new evidence from geochemical proxies. Quat. Int. 308–309, 89–104.
Harris, W.V., 2013. Defining and detecting Mediterranean deforestation, 800BCE to 700CE. In: Harris (Ed.), The Ancient Mediterranean Environment between Science and History, pp. 173–194. Brill Collections: Classical Studies E-Books Online, Collection 2013.
Hatté, C., Morvan, J., Noury, C., Paterne, M., 2001. Is classical acid–alkali–acid treatment responsible for contamination? An alternative proposition. Radiocarbon 43, 177–182.
Heiri, O., Lotter, A., Lemcke, G., 2001. Loss on ignition as a method for estimating organic and carbonate content in sediments: reproducibility and comparability of results. J. Paleolimnol. 25, 101–110.
Hughes, J.D., 2011. Ancient deforestation revisited. J. Hist.Biol. 44 (1), 43–57.
Hurrell, J.W., 1995. Decadal trends in the North Atlantic Oscillation: regional temperatures and precipitation. Science 269 (5224), 676–679.
Joannin, S., Brugiapaglia, E., Beaulieu, J.L.D., Bernardo, L., Magny, M., Peyron, O., Vannière, B., 2012. Pollen-based reconstruction of Holocene vegetation and climate in Southern Italy: the case of Lago di Trifoglietti. Clim. Past Discuss. 8 (3), 2223–2279.
Joannin, S., Magny, M., Peyron, O., Vannière, B., Galop, D., 2014. Climate and land-use change during the late Holocene at Lake Ledro (southern Alps, Italy). Holocene 24 (5), 591–602.
Kaltenrieder, P., Procacci, G., Vannière, B., Tinner, W., 2010. Vegetation and fire history of the Euganean Hills (Colli Euganei) as recorded by Lateglacial and Holocene sedimentary series from Lago della Costa (northeastern Italy). Holocene 20 (5), 679–695.
Kaplan, J.O., Krumhardt, K.M., Zimmermann, N., 2009. The prehistoric and preindustrial deforestation of Europe. Quat. Sci. Rev. 28, 3016–3034.
Kirschvink, J.L., 1980. The least-squares line and plane and the analysis of paleomagnetic data. Geophys. J. R. Astron. Soc. 62, 699–718.
Köhler, E., Lange, E., 1979. A contribution to distinguish cereal from wild grass pollen grains by LM and SEM. Grana 18, 133–140.
Korte, M., Constable, C., Donadini, F., Holme, R., 2011. Reconstructing the Holocene geomagnetic field. Earth Planet. Sci. Lett. 312 (3), 497–505.
Kylander, M.E., Ampel, L., Wohlfarth, B., Veres, D., 2011. High-resolution X-ray fluorescence core scanning analysis of Les Echets (France) sedimentary sequence: new insights from chemical proxies. J. Quat. Sci. 26 (1), 109–117.
Ladurie, E. LeRoy, 1971. Times of Feast, Times of Famine: a History of Climate since the Year 1000 (Barbara Bray, Trans.). Doubleday and Company, Inc., New York, 426 pp.
Lavrieux, M., Jacob, J., Disnar, J.R., Bréheret, J.G., Le Milbeau, C., Miras, Y., Andrieu-Ponel, V., 2013. Sedimentary cannabinol tracks the history of hemp retting. Geology 41 (7), 751–754.
Leggio, T., 1989b. Le fortificazione di Rieti dall' altomedievo al Rinascimento (sec. VI–XVI). In: Quaderni di storia urbana et territoriali, vol. 4, pp. 18–27. Rieti.
Leggio, T., 1994. Momenti della riforma cistercense nella Sabina e nel Reatino tra XII e XIII secolo. Riv. Stor. Lazio 2, 17–61.
Leggio, T., 1995a. Trasformazioni del paesaggio dei monti Sabini dall'età romana al medioevo. In: Leggio, T., Marini, M. (Eds.), Il paesaggio della conca reatina. Problemi ed esperienze di una ricerca multidisciplinare, pp. 51–70. Rieti.
Leggio, T., 1995b. L'olivo e la Sabina tra età romana e medioevo. In: L'olivo in Sabina e nel Lazio. Storia e prospettive di una presenza colturale, Roma, pp. 13–77.
Leggio, T., 1998. Un difficile rapporto tra uomo e ambiente: il paesaggio della conca reatina tra boschi ed acque. In: Grillotti di Giacomo, M.G., Moretti, L. (Eds.), I valori dell'agricoltura nel tempo e nello spazio, vol. I. Brigati, pp. 99–115.
Leggio, T., 2000. Il territorio della Provincia di Rieti tra la tarda antichità e lo scorcio del Medioevo. Riv. Stor. Lazio Quad. VIII (3), 27–43.
Leggio, T., 2007. Pesca ed acque nel medioevo reatino. Riserva Naturale dei Laghi Lungo e Ripasottile, Rieti, p. 67.
Leggio, T., Serva, L., 1991. La bonifica della Piana di Rieti dall'età romana al Medioevo: influenze sui mutamenti del paesaggio. Not. dell'Enea 25–26, 61–70.
Leone, A., 2004. In: Angeli, Franco (Ed.), Ambiente e territorio agroforestale: linee guida per la pianificazione sostenibile e gli studi di impatto ambientale, vol. 95.
Lo Cascio, E., Malanima, P., 2005. Cycles and stability. Italian population before the demographic transition (225 B.C.-A.D. 1900). Riv. Storia Econ. XXI (3), 5–40.
López-Moreno, J., Vicente-Serrano, S., Móran-Tejeda, E., Lorenzo-Lacruz, J., Kenawy, A., Beniston, M., 2011. Effects of the North Atlantic Oscillation (NAO) on combined temperature and precipitation winter modes in the Mediterranean mountains: observed relationships and projections for the 21st century. Glob. Planet. Change 77, 62–76.
Lorenzetti, R., 1989. Studi e materiali per una Storia Sociale e Economica della Sabina. Ricerca dell'Istituto Eugenio Cirese promossa dalla Regione Lazio Assessorato alla Cultura, Rieti.
Lorenzetti, R., 1990. Lacus Velinus. Per la salubrità dell'aere et per l'abundantia. In: La bonifica dell'agro reatino dall'antico Lacus Velinus alla riorganizzazione del territorio, Milano.
Lorenzetti, R., 1994. La Sabina. Il territorio di carta, Roma.
Lorenzetti, R., 2009. La terra e le acque. Trasformazioni e persistenze del paesaggio della Valle Reatina, Rieti.
Magri, D., 2007. Advances in Italian palynological studies: late Pleistocene and Holocene records. J. Geol. Soc. Swed. 129 (4), 337–344.
McCormick, M., Buntgen, U., Cane, M., Cook, E., Harper, K., Huybers, P., Litt, T., Manning, S., Mayewski, A., More, A., Nicolussi, K., Tegel, W., 2012. Climate change during and after the Roman Empire: reconstructing the past from scientific and historical evidence. J. Interdiscip. Hist. 43 (2), 169–220.
McNeil, J.R., 1992. Mountains of the Mediterranean World: an Environmental History. Cambridge University Press, Cambridge.
Mercuri, A.M., Accorsi, C.A., Mazzanti, M.B., 2002. The long history of *Cannabis* and its cultivation by the Romans in central Italy, shown by pollen records from Lago Albano and Lago di Nemi. Veg. Hist. Archaeobot. 11 (4), 263–276.
Messedaglia, L., 1927. Il mais e la vita rurale italiana: saggio di storia agraria. Federazione italiana dei consorzi agrari.
Moriondo, M., Trombi, G., Ferrise, R., et al., 2013. Olive trees as bio-indicators of climate evolution in the Mediterranean Basin. Glob. Ecol. Biogeogr. 22 (7), 818–833.
Munoz, S., Gajewski, K., Peros, M.C., 2010. Synchronous environmental and cultural change in prehistory of the northeastern United States. PNAS 107 (51), 22008–22013.
Nalepka, D., Walanus, A., 2003. Data processing in pollen analysis. Acta Palaeobot. 43, 125–134.
Naspi, N., 2010. Il capitolo della Cattedrale nella vita economica e sociale della *civitas* reatina (PhD thesis). Università degli Studi di Sassari.
Newnham, R.M., Vanderfoes, M.J., Garnett, M.H., Lowe, D.J., Prior, C., Almond, P.C., 2007. Test of AMS 14C dating of pollen concentrates using tephrochronology. J. Quat. Sci. 22 (1), 37–51. http://dx.doi.org/10.1002/jqs.1016.
Nigrisoli, G., 1857. Rivista dei più importanti prodotti naturali e manifatturieri dello Stato Pontificio. Tipografia Governativa Taddei, Ferrara.
O'Sullivan, P., 2008. The 'collapse' of civilizations: what paleoenvironmental reconstruction cannot tell us, but anthropology can. Holocene 18 (1), 45–55.
Parotto, M., Praturlon, A., 1975. In: Ogniben, L., Parotto, M., Praturlon, A. (Eds.), Geological Summary of Central Apennines, Structural Model of Italy. Quad. Ric. Sci. 90, 257–306.
Pavón-Carrasco, F.J., Osete, M.L., Torta, J.M., Gaya-Piqué, L.R., 2009. A regional archeomagnetic model for Europe for the last 3000 years, SCHA.DIF.3K: applications to archeomagnetic dating. Geochem. Geophys. Geosyst 10, Q03013. http://dx.doi.org/10.1029/2008GC002244.

Piovesan, G., Schirone, B., 2000. Winter North Atlantic oscillation effects on the tree rings of the Italian beech (Fagus sylvatica L.). Int. J. Bio-Meteorol. 44 (3), 121–127.
Piovesan, G., Biondi, F., Bernabei, M., Di Filippo, A., Schirone, B., 2005. Spatial and altitudinal bioclimatic zones of the Italian peninsula identified from a beech (*Fagus sylvatica* L.) tree-ring network. Acta Oecol. 27 (3), 197–210.
Punt, W., Malotaux, M., 1984. The Northwest European Pollen Flora, 31. Cannabaceae, Moraceae and Urticaceae. Rev. Palaeobot. Palynol. 42, 23–44.
Punt, W., Johanna, A.A.B., Hoen, P.P., 1991. The Northwest European Pollen Flora, 45 Oleaceae. Rev. Palaeobot. Palynol. 69, 23–47.
R Core Team, 2012. R: a Language and Environment for Statistical Computing. R Foundation for Statistical Computing, Vienna, Austria, ISBN 3-900051-07-0. http://www.R-project.org/.
Reimer, P., Bard, E., Bayliss, A., Beck, J.W., Blackwell, P.G., Bronk Ramsey, C., Buck, C.E., Cheng, H., Edwards, R.L., Friedrich, M., Grootes, P.M., Guilderson, T.P., Haflidason, H., Hajdas, I., Hatt, C., Heaton, T.J., Hogg, A.G., Hughen, K.A., Kaiser, K.F., Kromer, B., Manning, S.W., Niu, M., Reimer, R.W., Richards, D.A., Scott, E.M., Southon, J.R., Turney, C.S.M., van der Plicht, J., 2013. IntCal13 and MARINE13 radiocarbon age calibration curves 0–50000 years calBP. Radiocarbon 55 (4), 1869–1887.
Riccardi, R., 2006. Studi geografici sui laghi L:ungo, Ripasottile e Ventina. In: Quaderni della Riserva Naturale dei laghi Lungo e Ripasottile, vol. 1, p. 47.
Roberts, A.P., 2006. High-resolution magnetic analysis of sediment cores: strengths, limitations and strategies for maximizing the value of long-core magnetic data. Phys. Earth Planet. Int. 156, 162–178.
Roberts, N., Stevenson, A.D., Davis, B., Cheddadi, R., Brewer, S., Rosen, A., 2004. Holocene climate, environment and cultural change in the circum-Mediterranean region. In: Battarbee, R.W., Gasse, F., Stickley, C.E. (Eds.), Past Climate Variability through Europe and Africa. Klewer Academic Publishers, Dordrecht, pp. 343–362 (Developments in Paleoenvironmental Research).
Rull, V., Vegas-Vilarrúbia, T., 2014. Preliminary report on a mid-19th century *Cannabis* pollen peak in NE Spain: historical context and potential chronological significance. Holocene, 0959683614540964.
Russo Ermolli, E., di Pasquale, G., 2002. Vegetation dynamics of south-western Italy in the last 28 kyr inferred from pollen analysis of a Tyrrhenian Sea core. Veg. Hist. Archaeobot. 11 (3), 211–220.
Russo Ermolli, E., Romano, P., Ruello, M.R., Barone Lumaga, M.R., 2014. The natural and cultural landscape of Naples (southern Italy) during the Graeco-Roman and Late Antique periods. J. Archaeol. Sci. 42, 399–411.
Russo Ermolli, E., Di Donato, V., Martín-Fernández, J.A., Orain, R., Lebreton, V., Piovesan, G., 2014. Vegetation patterns in the Southern Apennines (Italy) during MIS 13: deciphering pollen variability along a NW-SE transect. Rev. Palaeobot. Palynol. http://dx.doi.org/10.1016/j.revpalbo.2014.11.004 (in press).
Sabbatani, S., 2005. Tentativi di lotta al paludismo e alla malaria nel Medio Evo. Ruolo dei Monaci Benedettini e Cistercensi nella nascita della Medicina Monastica e nelle bonifiche ambientali nel Medio Evo. Le infezioni Med. 3, 196–207.
Sadori, L., Guardini, M., 2007. Charcoal analysis, a method to study vegetation and climate of the Holocene: the case of Lago di Pergusa (Sicily, Italy. Geobios 40, 173–180.
Sadori, L., Jahns, S., Peyron, O., 2011. Mid-Holocene vegetation history of the central Mediterranean. Holocene 21 (1), 117–129.
Sadori, L., Ortu, E., Peyron, O., Zanchetta, G., Vannière, B., Desmet, M., Magny, M., 2013. The last 7 millennia of vegetation and climate changes at Lago di Pergusa (central Sicily, Italy). Clim. Past 9 (4), 1969–1984.
Sagnotti, L., 2013. Demagnetization analysis in Excel (DAIE) – an open source workbook in Excel for viewing and analyzing demagnetization data from paleomagnetic discrete samples and u-channels. Ann. Geophys. 56 (1), D0114. http://dx.doi.org/10.4401/ag-6282.
Sagnotti, L., Rochette, P., Jackson, M., Vadeboin, F., Dinarès-Turell, J., Winkler, A., 2003. Inter-laboratory calibration of low-field magnetic and anhysteretic susceptibility measurements. Phys. Earth Planet. Inter. 138 http://dx.doi.org/10.1016/S0031-9201(03)00063-3.
Sereni, E., 1973. Agricoltura e mondo rurale. In: Einaudi, Torino (Ed.), Storia d'Italia, I, I caratteri originali, pp. 133–252.
Sisani, S. (Ed.), 2009. Nursia e l'ager Nursinus. Un distretto sabino dalla *praefectura al municipium* (catalogue of the exhibition, Norcia 2009). Quasar, Roma.
Sköld, E., Lagerås, P., Berglund, B.E., 2010. Temporal cultural landscape dynamics in a marginal upland area: agricultural expansions and contractions inferred from palynological evidence at Yttra Berg, southern Sweden. Veg. Hist. Archaeobot. 19, 121–136.
Soligo, M., Tuccimei, P., Barberi, R., Delitala, M.C., Miccadei, E., Taddeucci, A., 2002. U/Th dating of freshwater travertine from Middle Velino Valley (Central Italy): paleoclimatic and geological implications. Palaeogeogr. Palaeoclimatol. Paleoecol. 184, 147–161.
Spadoni, M., Brilli, M., Giustini, F., Petitta, M., 2010. Using GIS for modelling the impact of current climate trend on the recharge area of the S. Susanna spring (sentral Apennines, Italy). Hydrol. Process 24, 50–64.
Stockmarr, J., 1971. Tablets with spores used in absolute pollen analysis. Pollen Spores 13, 615–621.
Sulpizio, R., Zanchetta, G., Caron, B., Dellino, P., Mele, D., Giaccio, B., Insinga, D., Paterne, M., Siani, G., Costa, A., Macedonio, G., Santacroce, R., 2014. Volcanic ash hazard in the central Mediterranean assessed from geological data. Bull. Volcanol. 76, 866–874.
Tennant, R.K., Jones, R.T., Brock, F., Cook, C., Turney, C.M., Love, J., Lee, R., 2013. A new flow cytometry method enabling rapid purification of fossil pollen from terrestrial sediments for AMS radiocarbon dating. J. Quat. Sci. http://dx.doi.org/10.1002/jqs.2606.
Tinner, W., van Leeuwen, J., Colombaroli, D., Vescovi, E., van der Knaap, W., Henne, P., Pasta, S., D'Angelo, S., Mantia, T., 2009. Holocene environmental and climatic changes at Gorgo Basso, a coastal lake in southern Sicily, Italy. Quat. Sci. Rev. 28, 1498–1510.
Tozzi, I., 2009. I riti funebri ed il pietoso ufficio della sepoltura a Rieti durante l'età moderna. Storia del mondo 59.
Trachsel, M., Kamenik, C., Grosjean, M., McCarroll, D., Moberg, A., Brázdil, R., Riemann, D., 2012. Multi-archive summer temperature reconstruction for the European Alps, AD 1053–1996. Quat. Sci. Rev. 46, 66–79.
Trouet, V., Esper, J., Graham, N.E., Baker, A., Scourse, J.D., Frank, D.C., 2009. Persistent positive North Atlantic oscillation Mode dominated the medieval climate anomaly. Science 324, 78.
Van Benthem, F., Clarke, G.C.S., Punt, W., 1984. The Northwest European Pollen Flora, 33. Fagaceae. Rev. Palaeobot. Palynol. 42, 87–110.
van Geel, B., Aptroot, A., 2006. Fossil ascomycetes in Quaternary deposits. Nova Hedwig. 82, 313–329.
van Geel, B., Gelorini, V., Lyaruu, A., Aptroot, A., Rucina, S., Marchant, R., Sinninghe Damsté, J.S., Verschuren, D., 2011. Diversity and ecology of tropical African fungal spores from a 25,000-year palaeoenviromental record in southeastern Kenya. Rev. Palaeobot. Palynol. 164, 174–190.
van Hoof, T.B., Bunnik, F.P.M., Waucomont, J.G.M., Kürschner, W.M., Visscher, H., 2006. Forest re-growth on medieval farmland after the Black Death pandemic — implications for atmospheric CO_2 levels. Palaeogeogr. Palaeoclimatol. Palaeoecol. 237, 396–411.
Vecchio, B., 1974. In: Einaudi (Ed.), Il bosco negli scrittori italiani del Settecento e dell'età napoleonica. Torino.
Vogel, J.S., Southon, J.R., Nelson, D.E., Brown, T.A., 1984. Performance of catalytically condensed carbon for use in accelerator mass spectrometry. Nucl. Instrum. Methods B5, 289–293.
Yeloff, D., van Geel, B., 2007. Abandonment of farmland and vegetation succession following the Eurasian plague pandemic of AD 1347-52. J. Biogeogr. 34, 575–582.
Zuccagni-Orlandini, A., 1843. Corografia fisica, storica e statistica dell'Italia e delle sue isole: corredata di un Atalante di mappe geograf e topografiche, e di altre tavole illustrative, vol. 10. Firenze [2] Supplemento. Editori.